NASA/TM—2019-220019

Thermal System Sizing Comparison of a PEM and Solid Oxide Fuel Cell Systems on Mars

Anthony Colozza
Vantage Partners, LLC, Brook Park, Ohio

Ian Jakupca
Glenn Research Center, Cleveland, Ohio

February 2019

NASA STI Program . . . in Profile

Since its founding, NASA has been dedicated to the advancement of aeronautics and space science. The NASA Scientific and Technical Information (STI) Program plays a key part in helping NASA maintain this important role.

The NASA STI Program operates under the auspices of the Agency Chief Information Officer. It collects, organizes, provides for archiving, and disseminates NASA's STI. The NASA STI Program provides access to the NASA Technical Report Server—Registered (NTRS Reg) and NASA Technical Report Server—Public (NTRS) thus providing one of the largest collections of aeronautical and space science STI in the world. Results are published in both non-NASA channels and by NASA in the NASA STI Report Series, which includes the following report types:

- TECHNICAL PUBLICATION. Reports of completed research or a major significant phase of research that present the results of NASA programs and include extensive data or theoretical analysis. Includes compilations of significant scientific and technical data and information deemed to be of continuing reference value. NASA counter-part of peer-reviewed formal professional papers, but has less stringent limitations on manuscript length and extent of graphic presentations.

- TECHNICAL MEMORANDUM. Scientific and technical findings that are preliminary or of specialized interest, e.g., "quick-release" reports, working papers, and bibliographies that contain minimal annotation. Does not contain extensive analysis.

- CONTRACTOR REPORT. Scientific and technical findings by NASA-sponsored contractors and grantees.

- CONFERENCE PUBLICATION. Collected papers from scientific and technical conferences, symposia, seminars, or other meetings sponsored or co-sponsored by NASA.

- SPECIAL PUBLICATION. Scientific, technical, or historical information from NASA programs, projects, and missions, often concerned with subjects having substantial public interest.

- TECHNICAL TRANSLATION. English-language translations of foreign scientific and technical material pertinent to NASA's mission.

For more information about the NASA STI program, see the following:

- Access the NASA STI program home page at http://www.sti.nasa.gov

- E-mail your question to help@sti.nasa.gov

- Fax your question to the NASA STI Information Desk at 757-864-6500

- Telephone the NASA STI Information Desk at 757-864-9658

- Write to:
  NASA STI Program
  Mail Stop 148
  NASA Langley Research Center
  Hampton, VA 23681-2199

NASA/TM—2019-220019

Thermal System Sizing Comparison of a PEM and Solid Oxide Fuel Cell Systems on Mars

Anthony Colozza
Vantage Partners, LLC, Brook Park, Ohio

Ian Jakupca
Glenn Research Center, Cleveland, Ohio

National Aeronautics and
Space Administration

Glenn Research Center
Cleveland, Ohio 44135

February 2019

Level of Review: This material has been technically reviewed by technical management.

Available from

NASA STI Program
Mail Stop 148
NASA Langley Research Center
Hampton, VA 23681-2199

National Technical Information Service
5285 Port Royal Road
Springfield, VA 22161
703-605-6000

This report is available in electronic form at http://www.sti.nasa.gov/ and http://ntrs.nasa.gov/

Contents

Abstract 1
1.0 Background 1
2.0 Environment 4
3.0 Analysis and Sizing 11
    3.1 Radiator System 11
    3.2 Insulation 14
    3.3 Heat Exchangers 17
4.0 Sizing Results 22
    4.1 PEM Fuel Cell Thermal System Sizing Result 23
    4.2 Solid Oxide Fuel Cell Thermal System Sizing Result 26
5.0 Summary 30
References 30

Thermal System Sizing Comparison of a PEM and Solid Oxide Fuel Cell Systems on Mars

Anthony Colozza
Vantage Partners, LLC
Brook Park, Ohio 44142

Ian Jakupca
National Aeronautics and Space Administration
Glenn Research Center
Cleveland, Ohio 44135

Abstract

Power production is a key aspect to any Mars mission. One method for providing power throughout the day/night cycle, or to satisfy short-duration high-output power needs, is to utilize a regenerative fuel cell system for providing energy storage and nighttime or supplemental power. This study compares the total system mass for two types of fuel cell systems, proton exchange membrane (PEM) and solid oxide (SO), sized to provide 10 kW of electrical output power in the Mars environment. Two operating locations were examined; one near the equator at 4° S latitude and one the higher northern latitude of 48° N. The systems were sized to operate throughout the year at these locations, where the radiator was sized for the worst-case warm condition and the insulation was sized for the worst-case cold condition. Using the selected system parameters, the results for both latitudes showed that the lightest system was the SO fuel cell with a PEM electrolyzer. This was mainly due to the higher operational temperature of the SO system enabled a significantly smaller radiator mass compared to that of the PEM fuel cell system. However, there was a significant difference in mass for the PEM system when operated near the equator as compared to the higher northern latitude. For the 10-kW output system this difference in mass was just under 100 kg.

1.0 Background

Power production is a key aspect to any Mars exploration mission as reported in many NASA Mars architecture studies (Refs. 1 and 2). A manned mission to Mars will need a reliable energy storage system that can ensure power throughout the nighttime period. One energy storage approach is a regenerative fuel cell system. A regenerative fuel cell system operates in two phases like a rechargeable battery: charging and discharging. During the charging or energy storage phase, an external power source energizes an electrolyzer to generate and store a fuel and an oxidizer. These reactants are then utilized during the discharge, power production phase, to produce electrical power. The byproduct of the power production is stored for later use by and the electrolyzer to reconstitute the reactants, thereby continuing the cycle.

There are two feasible types of fuel cell/electrolyzers for this type of regenerative system on Mars; a proton exchange membrane (PEM) based system and a solid oxide (SO) based system. A general layout of this type of system is shown in Figure 1.

For this type of energy storage system to operate successfully within the Martian environment, the internal components must be maintained at their required operating temperature and the waste heat from the system needs to be rejected to the environment. For the purposes of this study, the steady-state electrical output power (P_e) of the regenerative fuel cell system is 10 kW. Not limited by the Carnot cycle, a fuel cell has an unattainable maximum theoretical efficiency of 83 percent based on the Gibbs

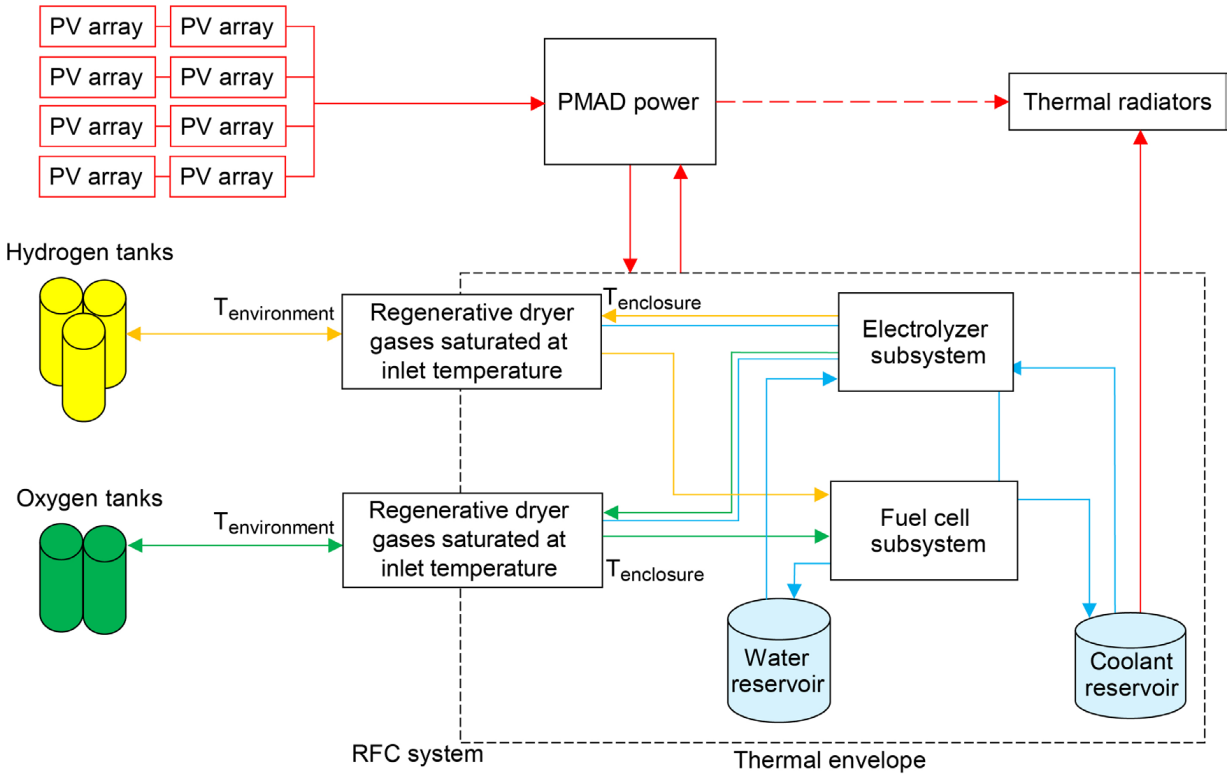

Figure 1.—RFC System general layout.

free energy conversion of hydrogen and oxygen to electricity heat and water (Ref. 3). The efficiencies listed in Table I are the quotient of the nominal average cell electrical potential (volts) over the thermal-neutral voltage of the $H_2 + ½O_2 \rightarrow H_2O$ reaction at the nominal operating temperature. The design current density was chosen to optimize system efficiency to minimize thermal loads and reactant mass. These fuel cell operating conditions are listed in Table I for both the PEM and SO systems. The waste heat (Q_{TH}) generated is based on the fuel cell efficiency (η_{fc}) as given by Equation (1).

$$Q_{TH} = P_e\left(\frac{1}{\eta_{fc}} - 1\right) \tag{1}$$

The thermal system will be utilized to maintain the system components within the required operating temperature range. This is accomplished by insulating the components to isolate them from the environment and rejecting the excess heat from the system to the environment. The main system layout is similar for both the PEM and solid oxide systems. The fuel cells subsystems are treated as interchangeable parts of the larger system as illustrated in Figure 2.

TABLE I.—FUEL CELL OPERATING PARAMETERS

Fuel cell type	Electrical power output, kW	Thermal-neutral potential, V_{dc}	Nominal cell potential, V_{dc}	Stack operating efficiency (Ref. 4)	Waste heat generated (Q_{TH}), kW	Operating temperature, °C
PEM	10	1.48	0.89	0.60	6.7	80
Solid oxide	10	1.36	1.02	0.75	3.33	750

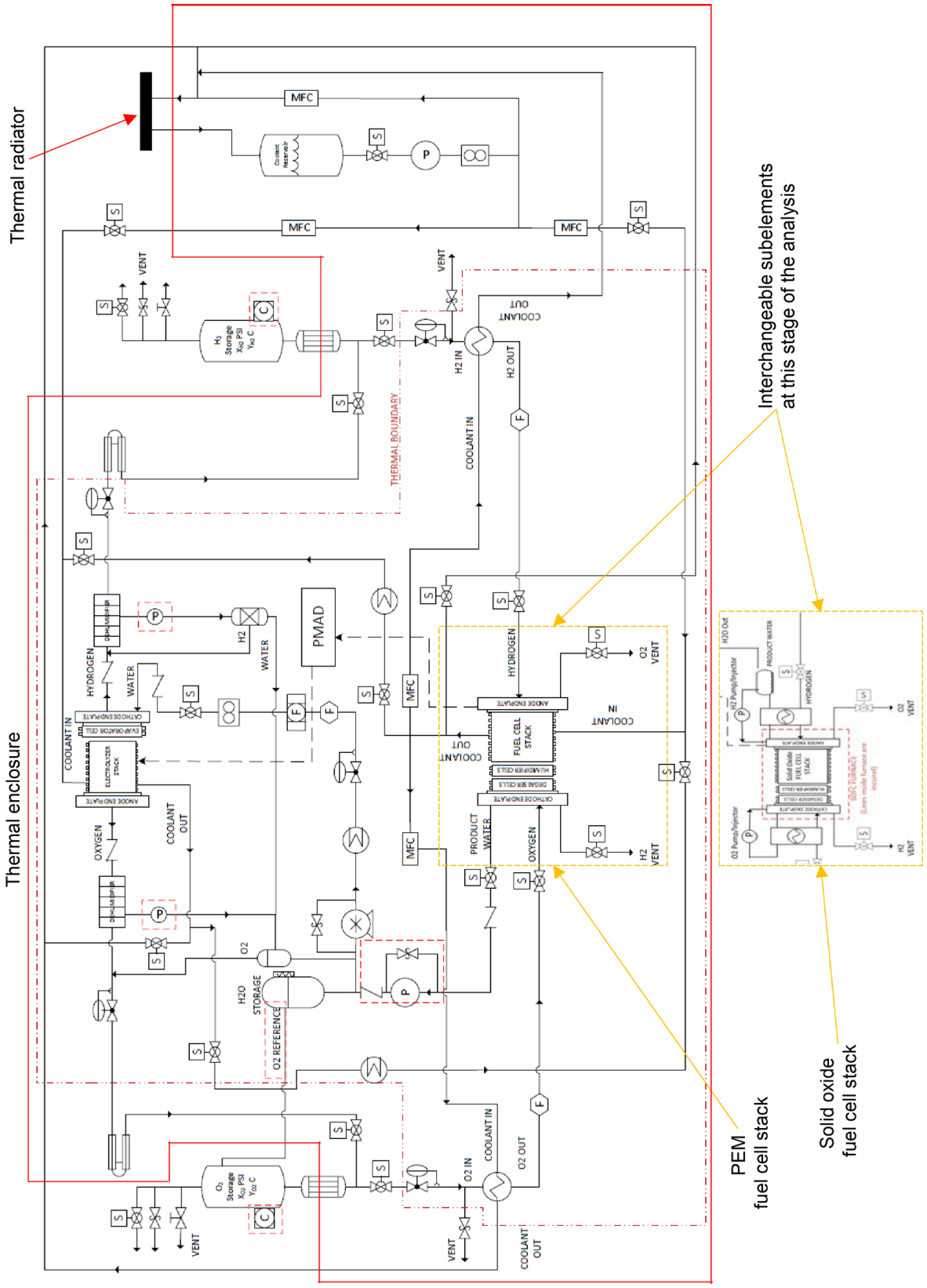

Figure 2.—Fuel cell power system layout.

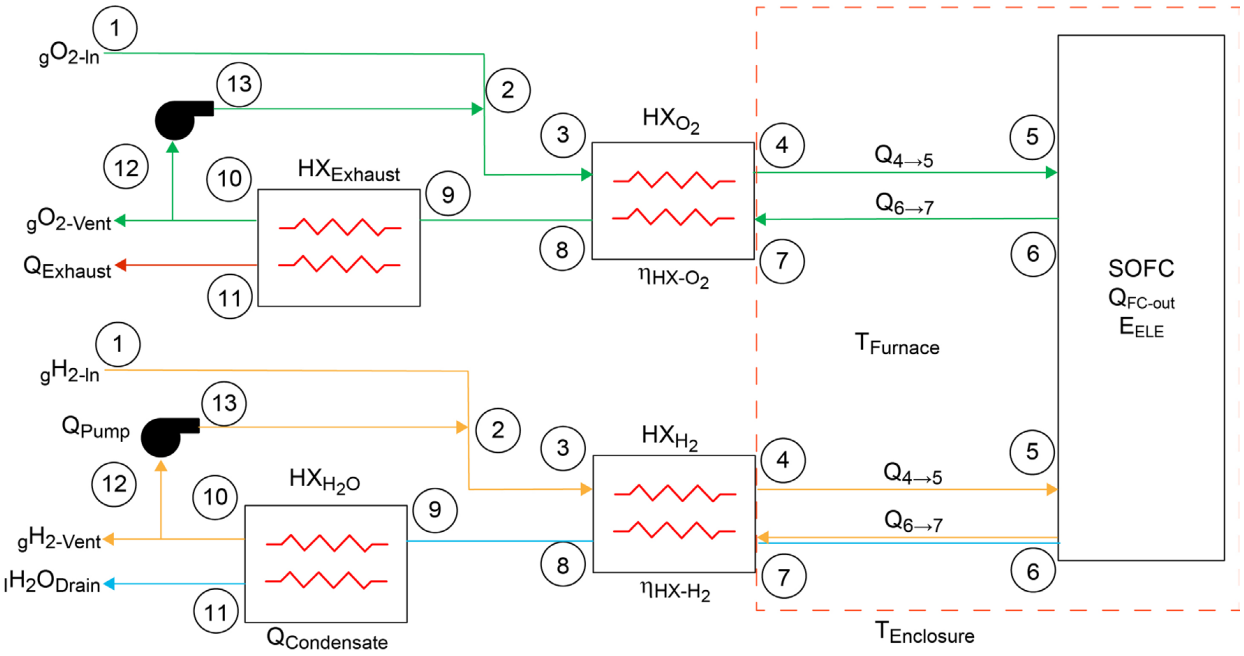

Figure 3.—Solid oxide fuel cell heat exchanger layout.

Because of the high temperature operation of the solid oxide fuel cell, a number of heat exchangers are needed to condition the reactant gases. This includes recovering some of the waste heat produced from the fuel cell to pre-heat the make-up reactants, thereby increasing the overall system efficiency. Preheating the reactant gas has the added benefit of reducing any temperature gradients within the fuel cell stack thereby reducing thermal stresses and increasing its operational lifetime. The heat exchanger layout for the solid oxide fuel cell is illustrated in the “Solid Oxide Fuel Cell” box shown in Figure 3.

2.0 Environment

From a thermal perspective, the environment on Mars is unique. The atmosphere on Mars near the surface is rarefied, similar to the air density on Earth at 30 km (~100,000 ft). Unlike on the surface of Earth, this low-density atmosphere limits convection heat removal which makes radiation the dominant heat transfer mechanism within the Mars surface environment. However, to accurately access a thermal system, convection still must be considered as the convective heat transfer contribution is not negligible. The atmosphere influences the selection of components for the thermal system. For example, in vacuum multi-layer insulation (MLI) is ideal and provides excellent insulating properties by blocking radiation heat transfer. But on Mars, the atmosphere greatly reduces the effectiveness of MLI so other types of insulation, such as aerogels, are utilized. The secondary atmospheric effect of dust transport onto a radiator panel degrades its emissivity over time. This degradation mechanism has to be considered in the design process or mitigated.

Accurately characterizing the Mars surface environment critically influences the design and sizing of the thermal system. Since the Mars atmosphere is mainly carbon dioxide, as given in Table II, the atmospheric properties can be approximated by those for CO_2 at the low Mars surface pressure.

TABLE II.—MARS ATMOSPHERIC COMPOSITION (REF. 5)

Gas	Abundance (by volume), %
Carbon dioxide (CO_2)	95.32
Nitrogen (N_2)	2.70
Argon (Ar)	1.6
Oxygen (O_2)	0.13
Carbon monoxide (CO)	0.08
Trace gasses: water (H_2O), nitrogen oxide (NO), neon (Ne), Hydrogen-deuterium-oxygen (HDO), krypton (Kr), xenon (Xe)	0.17

TABLE III.—VISCOSITY CALCULATION COEFFICIENTS (REF. 6)

Coefficient	Value
a_0	0.235156
a_1	–0.491266
a_2	0.05211155
a_3	0.05347906
a_4	–0.01537102

The dynamic viscosity (μ) of the atmospheric can be determined as a function of the surface atmospheric temperature (T_{sur}) in Kelvin from Equations (2) and (3) (Ref. 6).

$$\mu = \frac{1.00697 \times 10^{-6} \sqrt{T_{sur}}}{e^{a}} \quad \text{[Pa·s]} \tag{2}$$

where

$$a = a_0 + a_1 \ln\frac{T_{sur}}{251.096} + a_2\left(\ln\frac{T_{sur}}{251.096}\right)^2 + a_3\left(\ln\frac{T_{sur}}{251.096}\right)^3 + a_4\left(\ln\frac{T_{sur}}{251.096}\right)^4 \tag{3}$$

The coefficients a_0 through a_4 are given in Table III.

The thermal conductivity (k) of the atmosphere can also be estimated as a function of the atmospheric temperature in Kelvin from Equations (4) to (6).

$$k = \frac{0.119421\sqrt{T_{sur}}\,(1+b)}{cT_{sur}} \quad \text{[W/mk]} \tag{4}$$

where

$$b = b_0 + \frac{251.096 b_1}{T_{sur}} + \frac{251.096^2 b_2}{{T_{sur}}^2} + \frac{251.096^3 b_3}{{T_{sur}}^3} + \frac{251.096^6 b_6}{{T_{sur}}^6} + \frac{251.096^7 b_7}{{T_{sur}}^7} \tag{5}$$

$$c = \sqrt{0.4 * \left(1 + e^{-183.5/T}\left(\frac{c_1 T_{sur}}{100} + c_2 + \frac{100 c_3}{T_{sur}} + \frac{100^2 c_4}{{T_{sur}}^2} + \frac{100^3 c_5}{{T_{sur}}^3}\right)\right)} \tag{6}$$

The b and c coefficients for the thermal conductivity calculation are given in Table IV.

TABLE IV.—THERMAL CONDUCTIVITY CALCULATION COEFFICIENTS (REF. 6)

b coefficient	*b* value	*c* coefficient	*c* value
b_0	0.4226159	c_1	0.02387869
b_1	0.6280115	c_2	4.350794
b_2	–0.5387661	c_3	–10.33404
b_3	0.6735941	c_4	7.98159
b_6	–0.4362677	c_5	–1.940558
b_7	0.2255388		

The specific heat (c_p) of the Mars atmosphere as a function of temperature can also be approximated with the specific heat of CO_2. For CO_2, the specific heat is fairly linear over the temperature range seen within the Mars environment (Ref. 7) as given by Equation (7).

$$c_p = 0.0011T_{sur} + 0.5177 \tag{7}$$

The atmospheric density at the surface can be determined from the ideal gas equation using the atmospheric temperature and pressure. This is given in Equation (7). For Mars, the gas constant for CO_2 (R_{CO_2}), 188.9 [J/kg·K], can be used to approximate the gas constant for the atmosphere (Ref. 8). The pressure (P) as well as the temperature on the surface varies throughout the year as shown in the Viking II lander data given in Figure 4 and Figure 5. The density (ρ) can then be calculated from the ideal gas equation based on the atmospheric temperature and pressure, as given by Equation (8).

$$\rho = \frac{P}{R_{\mathrm{CO}_2} T_{sur}} \tag{8}$$

Using the data from Figure 4 and Figure 5 and Equation (7), the variation in atmospheric density near the surface can be calculated is shown in Figure 6. The atmosphere density varies widely throughout the year ranging between 0.016 and 0.034 kg/m^3 with the daily variations from 0.02 to 0.025 kg/m^3.

The Viking II lander provided the highest latitude yearlong data for Mars temperature and pressure. The Mars Science Laboratory (MSL) Curiosity rover provided pressure and temperature data at a latitude of 4.36° S as shown in Figure 7.

As with the Viking II data, the atmospheric density at the MSL latitude can be determined from the pressure and temperature given in Figure 8 and Figure 9. The atmospheric density is shown in Figure 9. It has a maximum of 0.021 kg/m^3 and a minimum of 0.014 kg/m^3. With a maximum yearly variation of 33 percent which is significantly less variation than the higher latitude Viking II data.

The effective sky temperature (T_{sky}) is another required environmental property to accurately determine the radiative heat transfer to the surroundings. The sky temperature is difficult to calculate since it is dependent on a number of local factors, such as dust opacity, water vapor content, wind speed, etc., that can be highly variable for a given location and time of day/year. To estimate the effective sky temperature based on the surface temperature, a liner curve fit of the relationship between the worst-case surface and sky temperature (Ref. 9) was made and is given by Equation (9).

$$T_{sky} = 74.841 + 0.4185T_{sur} \ \text{[K]} \tag{9}$$

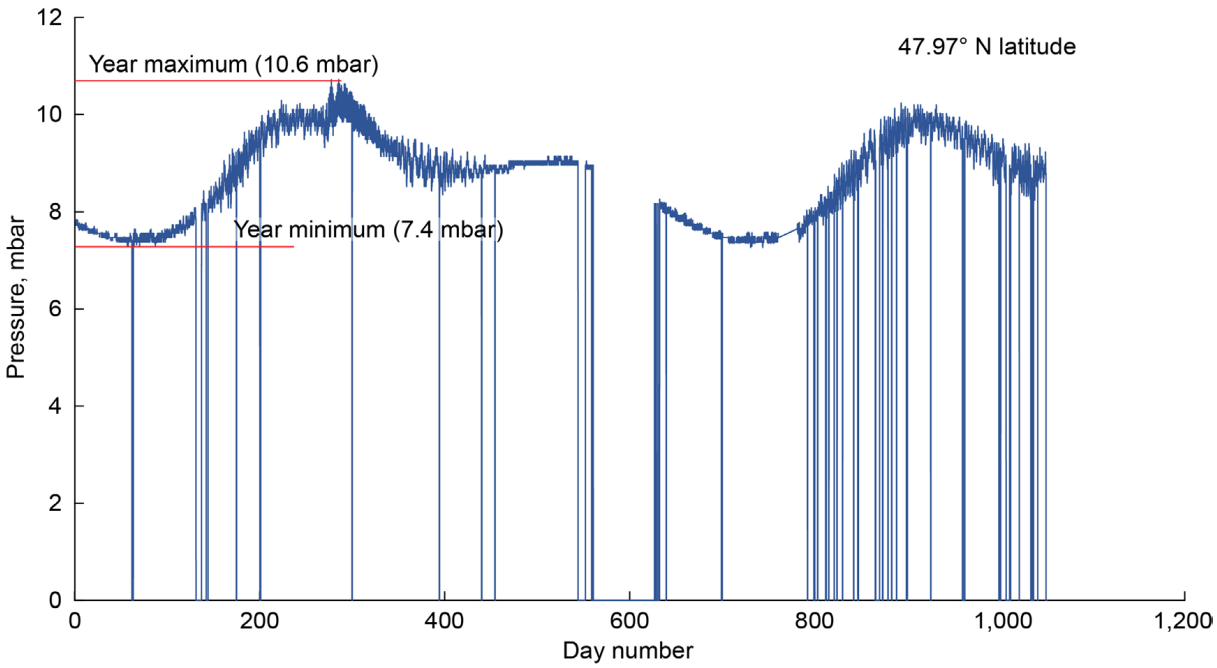

Figure 4.—Viking II lander surface pressure (Ref. 9).

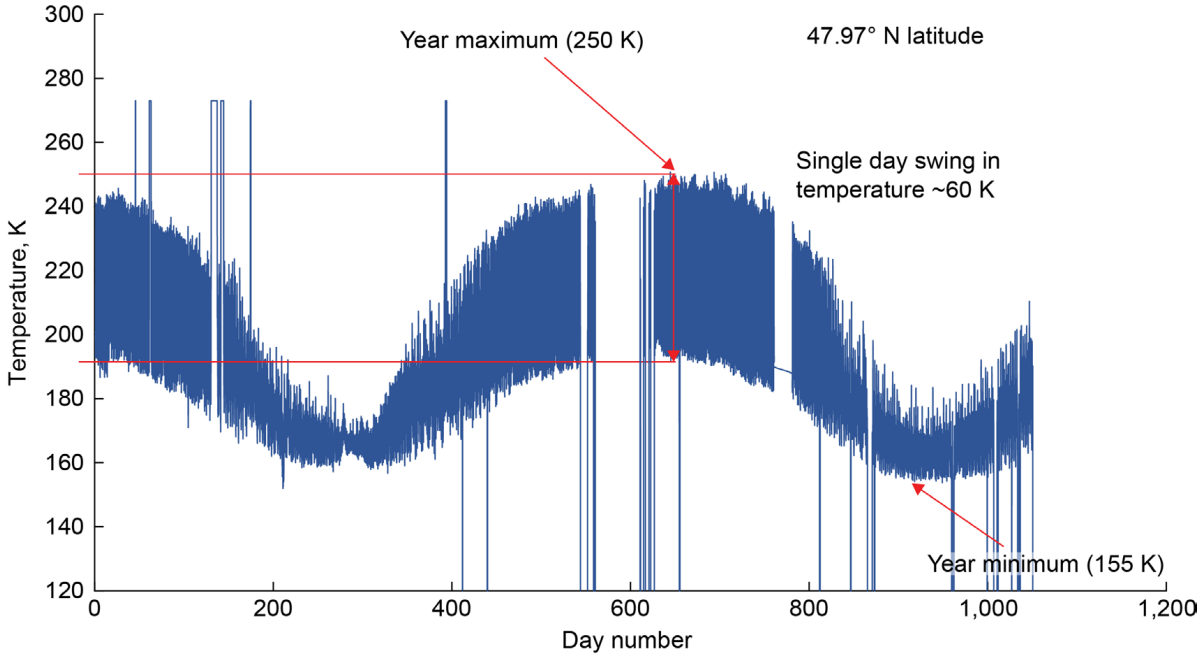

Figure 5.—Viking II lander surface temperature (Ref. 9).

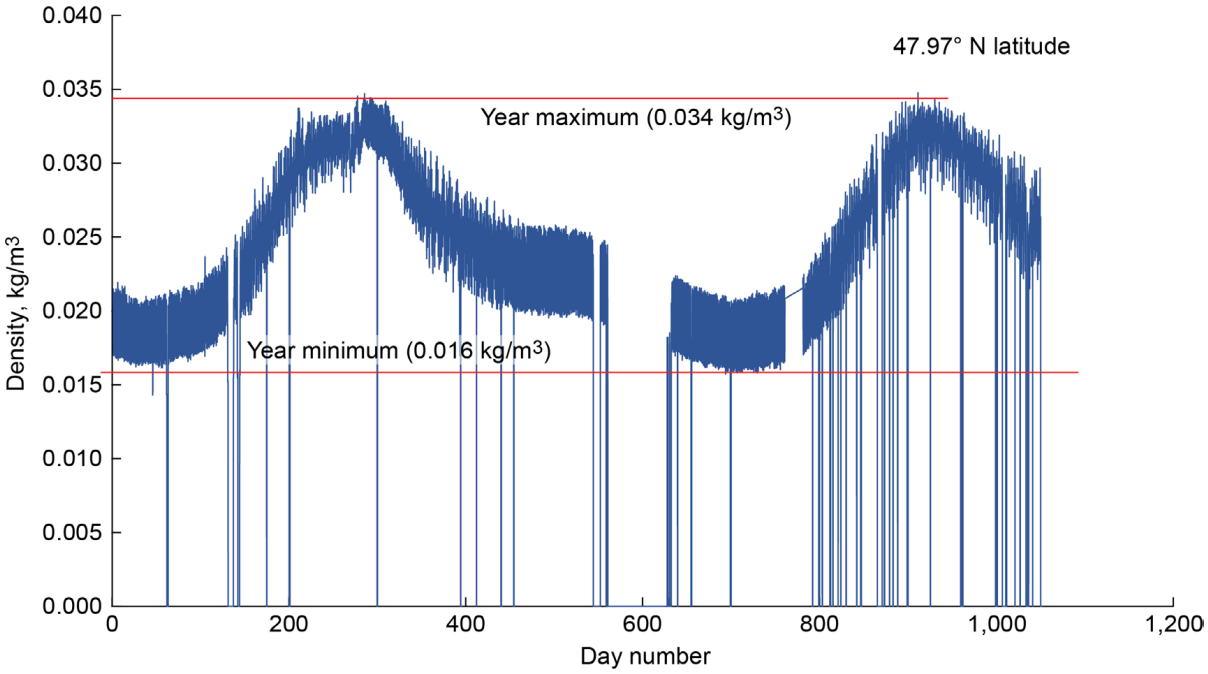

Figure 6.—Surface density based on Viking II data (Ref. 9).

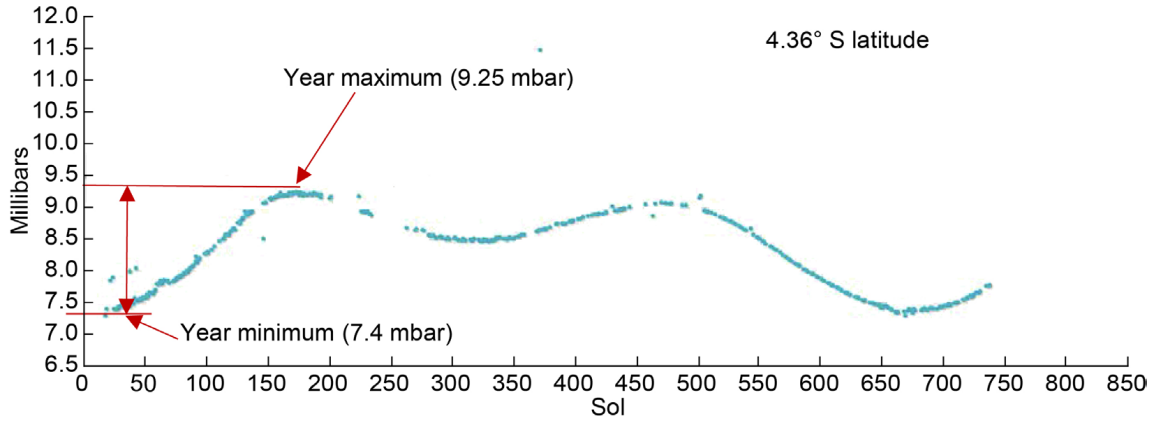

Figure 7.—MSL Curiosity rover surface pressure (Ref. 10).

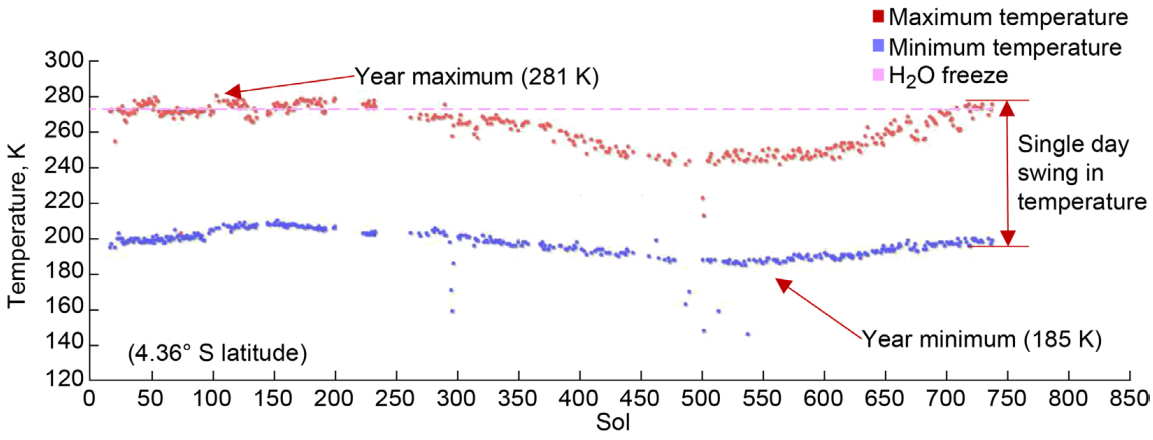

Figure 8.—MSL Curiosity rover surface temperature (Ref. 10).

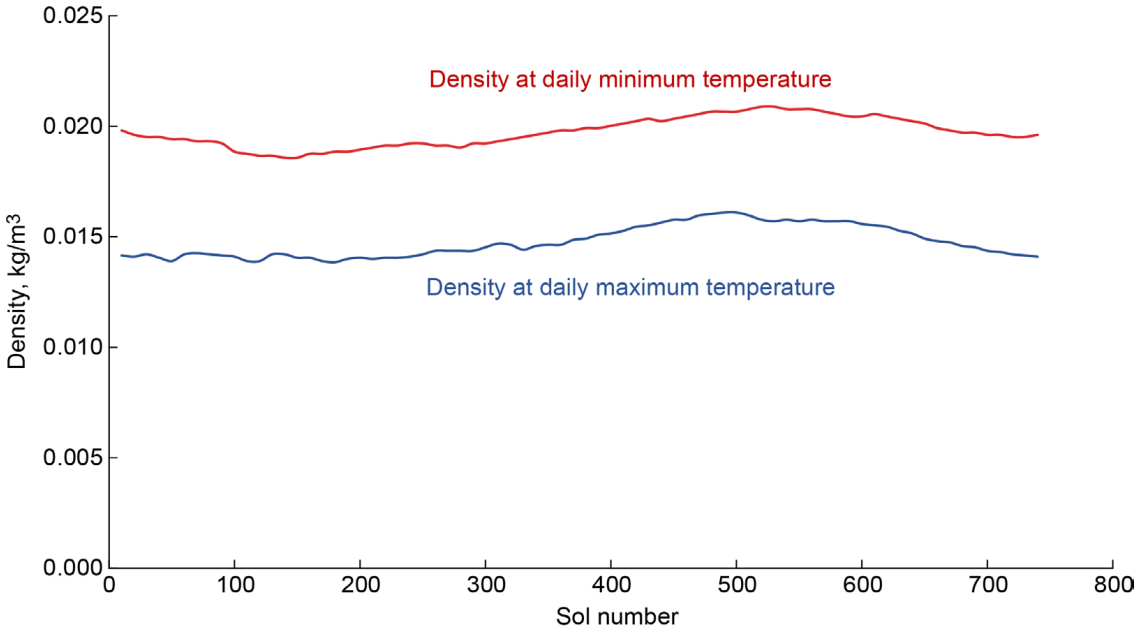

Figure 9.—Atmospheric density based on MSL data.

TABLE V.—ATMOSPHERE CHARACTERISTICS AT THE MARS SURFACE

Latitude	4.36° S		47.97° N	
Characteristic	Minimum temperature	Maximum temperature	Minimum temperature	Maximum temperature
Gravitational acceleration (Ref. 3), g	3.711 m/s^2			
Day of the year, sol	525	100	275	660
Surface temperature (T_{sur}), K	185	281	155	250
Density, kg/m^3	0.025	0.016	0.034	0.017
Specific Heat, J/kg·K	721.2	826.8	688.2	792.7
Dynamic viscosity, Pa·s	9.29×10^{-6}	1.15×10^{-5}	7.77×10^{-6}	9.88×10^{-6}
Thermal conductivity, W/m·K	0.013	0.016	0.010	0.013
Effective sky temperature, K	152.3	192.4	139.7	179.5

From the above equations and data, the atmospheric characteristics can be approximated for the worst case hot and cold conditions at both the upper and lower bounding latitudes of 47.97° N and 4.36° S. These characteristics for the Mars surface atmospheric conditions are given in Table V.

As mentioned previously, the wind velocity (V) is a key environmental factor. The wind speed at the Viking I and II landing sites is shown in Figure 10 and Figure 11, respectively. These profiles represent a higher and lower latitude wind distribution. The values for both sites had similar maximum and average wind speeds. The wind characteristics for both sites are summarized in Table VI.

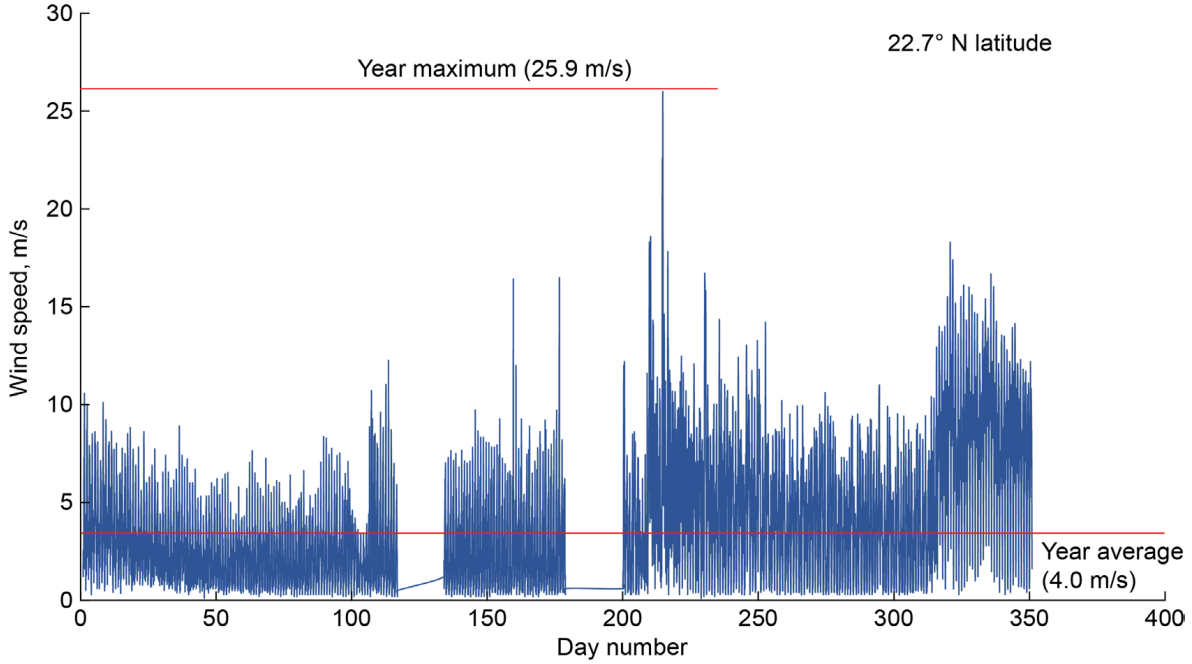

Figure 10.—Wind speed at the Viking I landing site (Ref. 9).

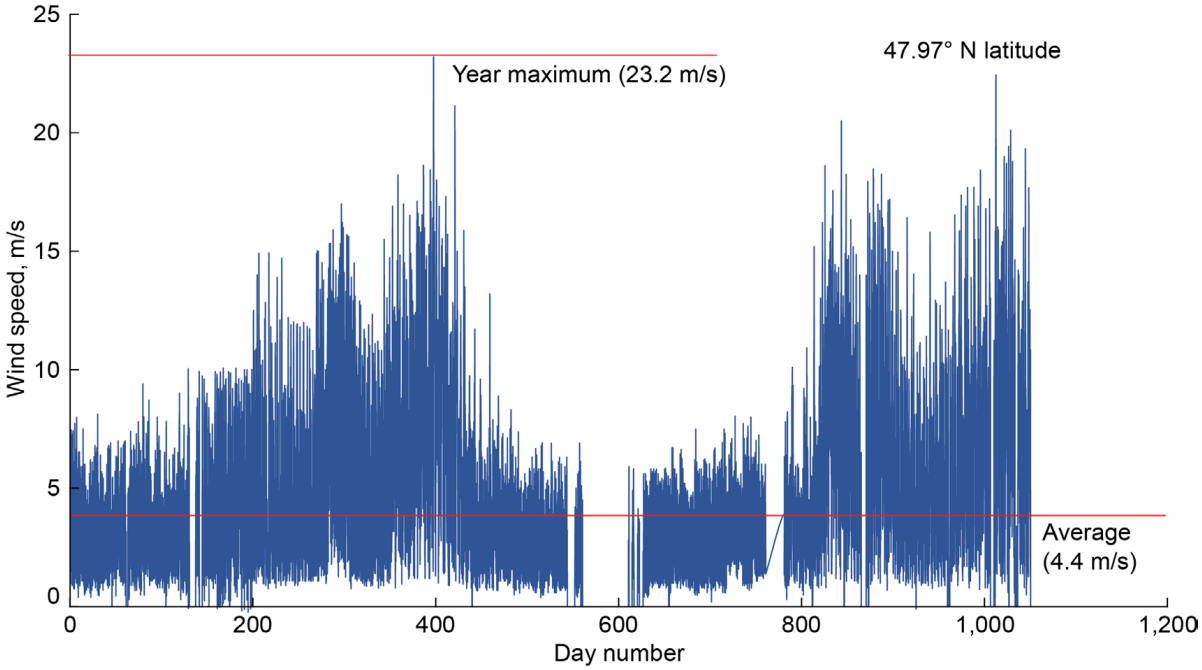

Figure 11.—Wind speed at the Viking II landing site (Ref. 9).

TABLE VI.—SURFACE WIND SPEED CHARACTERISTICS

Characteristic	Viking I (22.7° N), m/s	Viking II (47.97° N), m/s
Average	4.0	4.4
Maximum	25.9	23.2
Minimum	0.1	0.0
Median	3.2	3.4
Standard deviation	3.27	3.52

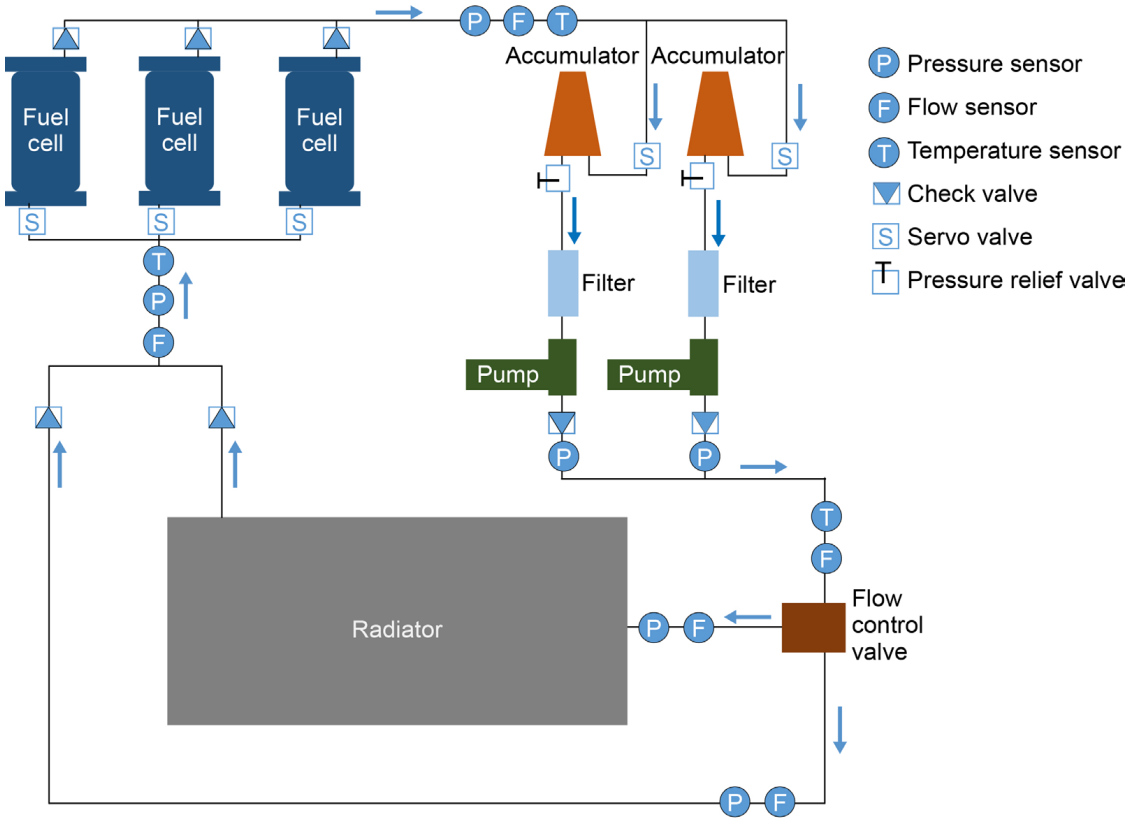

Figure 12.—Pump loop coolant system layout.

3.0 Analysis and Sizing

3.1 Radiator System

The fuel cell thermal control system is a pumped-loop system circulating a coolant which collect heat by flowing through the fuel cells, or fuel cell stack cold plates, to a radiator which rejects the waste heat to the environment. This configuration and the corresponding components are shown in Figure 12.

The sizing of the system is based on the heat load that has to be rejected and the heat transfer from the radiator to the surroundings. The heat transfer from the radiator is through both radiation and convection. Even though the atmosphere is rarefied, convection still plays a role in the heat removal from the radiator and therefore must be accurately modeled to correctly size the radiator.

The heat transfer from the radiator to the surroundings through convection (Q_c) is given by Equation (10). It is based on the radiator temperature (T_r) and area (A_r) as well as the local bulk atmosphere temperature (T_{atm}).

$$Q_c = A_r h\left(T_r - T_{atm}\right) \tag{10}$$

The convective coefficient (h) is given by Equation (11) which is based on the characteristic length (L) of the radiator.

$$h = \frac{\mathrm{Nu}\, k}{L} \tag{11}$$

The expression for the Nusselt number (Nu) will depend on whether the wind speed results in natural or forced convection from the radiator surface. These cases are given by Equation (12) for natural convection and Equations (13) and (14) for laminar or turbulent flow forced convection, respectively (Ref. 11). The transition between laminar to turbulent flow occurs at a Reynolds number (Re) of approximately 5×10^5.

$$\mathrm{Nu} = 0.68 + \frac{0.67\mathrm{Ra}^{1/4}}{\left[1+\left(\frac{0.492}{\mathrm{Pr}}\right)^{\frac{9}{16}}\right]^{4/9}} \quad \text{(natural convection)} \tag{12}$$

$$\mathrm{Nu} = \frac{0.3387\,\mathrm{Re}^{1/2}\,\mathrm{Pr}^{1/3}}{\left[1+\left(\frac{0.0468}{\mathrm{Pr}}\right)^{\frac{2}{3}}\right]^{1/4}} \qquad \text{(laminar flow)} \tag{13}$$

$$\mathrm{Nu} = 0.0296\,\mathrm{Re}^{4/5}\,\mathrm{Pr}^{1/3} \quad \text{(turbulent flow)} \tag{14}$$

The Nusselt number equations are based on the Prandtl number (Pr), Reynolds number (Re) and the Rayleigh number (Ra) given by Equations (15), (16), and (17), respectively(Ref. 11).

$$\mathrm{Pr} = \frac{c_p \mu}{k} \tag{15}$$

$$\mathrm{Re} = \frac{\rho V L}{\mu} \tag{16}$$

$$\mathrm{Ra} = \frac{g\left(T_r - T_a\right) L^3 \rho^2 c_p}{T_f \mu} \tag{17}$$

Where the film temperature (T_f) is assumed to be the average of the radiator temperature and the atmosphere temperature.

$$T_f = \frac{T_r + T_{atm}}{2} \tag{18}$$

Radiation heat transfer (Q_r) is the next and main means of heat transfer from the radiator. On the surface of Mars, the radiator has a view to both the surface (F_{sur}) and the sky (F_{sky}). These two views compose the total view of the radiator to the surroundings as given by Equation (19).

$$1 = F_{sur} + F_{sky} \tag{19}$$

The total radiative heat transfer from the radiator to the surface and sky is dependent on the emissivity of the radiator (ε) as given by Equation (20).

$$Q_r = A_r \varepsilon \sigma \left[F_{sky} \left(T_r^4 - T_{sky}^4 \right) + F_{sur} \left(T_r^4 - T_{sur}^4 \right) \right] \tag{20}$$

Where the Stefan-Boltzmann constant (σ) is:

$$\sigma = 5.670367 \times 10^{-8} \ [\mathrm{W/m^2K^4}] \tag{21}$$

Based on Equations (10) and (20), the total heat rejection capability of the radiator (Q) to the surroundings is given by Equation (22):

$$Q = Q_c + Q_r \tag{22}$$

An estimate of the mass of the radiator panel (m_r) can be made based on its required area. The radiator structure can be separated into the following components with a scaling coefficient for each component to linearly scale the mass based on the required radiator area: panels (C_p), coating (C_c), tubing (C_t), header (C_h), adhesives (C_a), stingers (C_s), and attachment (C_{at}). These coefficients were derived from satellite and spacecraft radiator mass data and are listed in Table VII. The total radiator mass is given by Equation (23).

$$m_r = C_p A_r + C_c A_r + C_t A_r + C_h A_r + C_a A_r + C_s A_r + C_{at} A_r \tag{23}$$

The cooling fluids for the thermal control system will vary greatly between the PEM fuel cell system and the solid oxide fuel cell system due to the large difference in the operating temperature. Because of the relatively low operating temperature of the PEM fuel cell a number of different cooling fluids can be used with the thermal control system. A number of potential fluids and their properties are given in Table VIII.

TABLE VII.—RADIATOR MASS SCALING COEFFICIENTS

Coefficient	Value, kg/m^2
C_p	3.3
C_c	0.42
C_t	1.31
C_h	0.23
C_a	0.29
C_s	1.50
C_{at}	0.75

TABLE VIII.—COOLING FLUIDS FOR PEM THERMAL SYSTEM (REF. 12 TO 16)

Fluid	Thermal conductivity, W/m·K	Specific heat, kJ/kg·K	Viscosity, MPa·s	Density, kg/m^3	Freezing point, °C	Boiling point, °C
Water	0.58	4.3	0.18	1,000	0	100
50-50 water ethylene glycol	0.402	3.9	0.37	1,082	–37	107
50-50 water propylene glycol	0.357	3.6	0.94	1,041	–45	106
CFC 11	0.05	1.0	0.16	1,485	–111	24
Dynalene HC-30	0.519	3.1	0.67	1,275	–40	112
Therminol 59	0.11	2.1	0.75	978	–45	289
Galden HT200	0.065	0.96	0.77	1,790	–85	200
Syltherm XLT	0.08	2.0	0.34	852	–111	260
Fluorinert FC-72	0.057	1.1	0.12	1,680	–90	56

TABLE IX.—COOLING FLUIDS FOR SOLID OXIDE THERMAL SYSTEM (REF. 17)

Fluid	Thermal conductivity, W/m·K	Specific heat, kJ/kg·K	Viscosity, MPa·s	Density, kg/m^3	Freezing point, °C	Boiling point, °C
Lithium	47.6	1.29	339	479	181	1,331
Mercury	10.0	0.042	1,141	13,231	–38.5	358
Potassium	36.6	0.235	169	714	64	761
Sodium	64.0	0.389	227	823	98.2	881
Na (22%), K (78%)	26.0	0.27	178	742	–11	784

For the solid oxide fuel cell system, the much higher operating temperature will utilize a liquid metal heat pipe cooling system. A list of potential coolants for the solid oxide system are given in Table IX.

3.2 Insulation

The evaluated thermal system utilizes aerogel insulation to minimize heat loss to the surroundings and maintain the internal component temperatures within the required range of 260 to 320 K.

Aerogel is a light-weight, open-cell insulation with a very low thermal conductivity of approximately 0.016 W/m·K. The cells within the aerogel constrain the natural convection of the atmospheric gas within the insulation. This enables a thermal conductivity to approach that of the atmospheric gas. Aerogel is comprised of silica gel and is available in a number of different densities, as illustrated in Figure 13. For this analysis, an aerogel density of 20 kg/m^3 is used.

Since the insulation lacks sufficient mechanical properties, an outer shell encases the insulation to prevent it from being crushed or damaged which would reduce its insulation properties. The aerogel insulation surrounds the enclosure containing all internal components for the fuel cell system that need to be within a controlled thermal environment.

The heat loss through the insulation is calculated by determining the enclosure surface temperature (T_{es}) and then calculating the heat flow through the insulation based on this temperature. The enclosure houses the electrical components of the system, as shown in Figure 2. The fuel cell is within the enclosure. The PEM fuel cell system will operate near the internal operating temperature of the enclosure

and therefore will not require thermal isolation from the system. The solid oxide fuel cell system will operate at a significantly higher temperature than the enclosure and will require additional insulation isolating it from the other components within the enclosure. It can be considered a separate segment of the enclosure with its own thermal requirements.

The heat flow through the enclosure insulation (Q_e) is dependent on the convective (Q_{ec}) and radiative heat transfer (Q_{er}) from the enclosure to the surroundings as given by Equation (24) and illustrated in Figure 14.

$$Q_e = Q_{ec} + Q_{er} \tag{24}$$

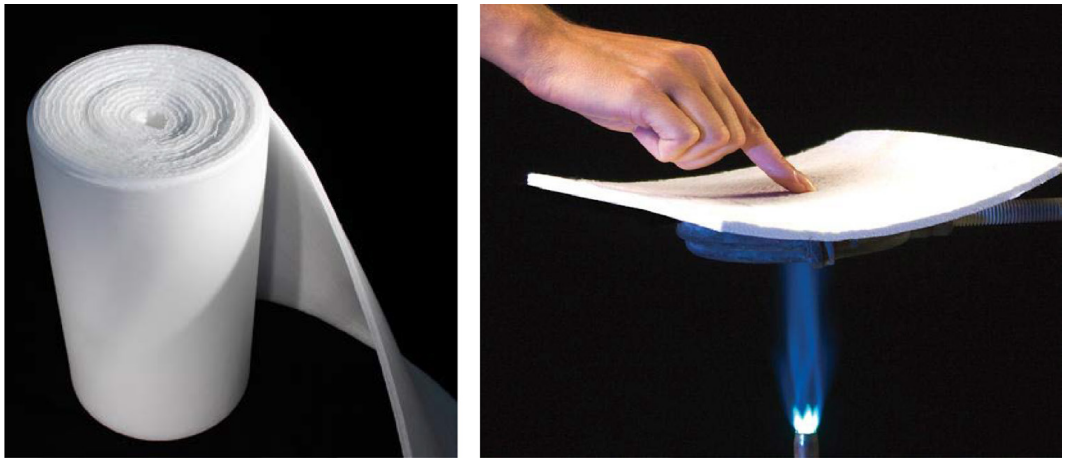

Figure 13.—Aerogel insulation examples (Refs. 18 and 19).

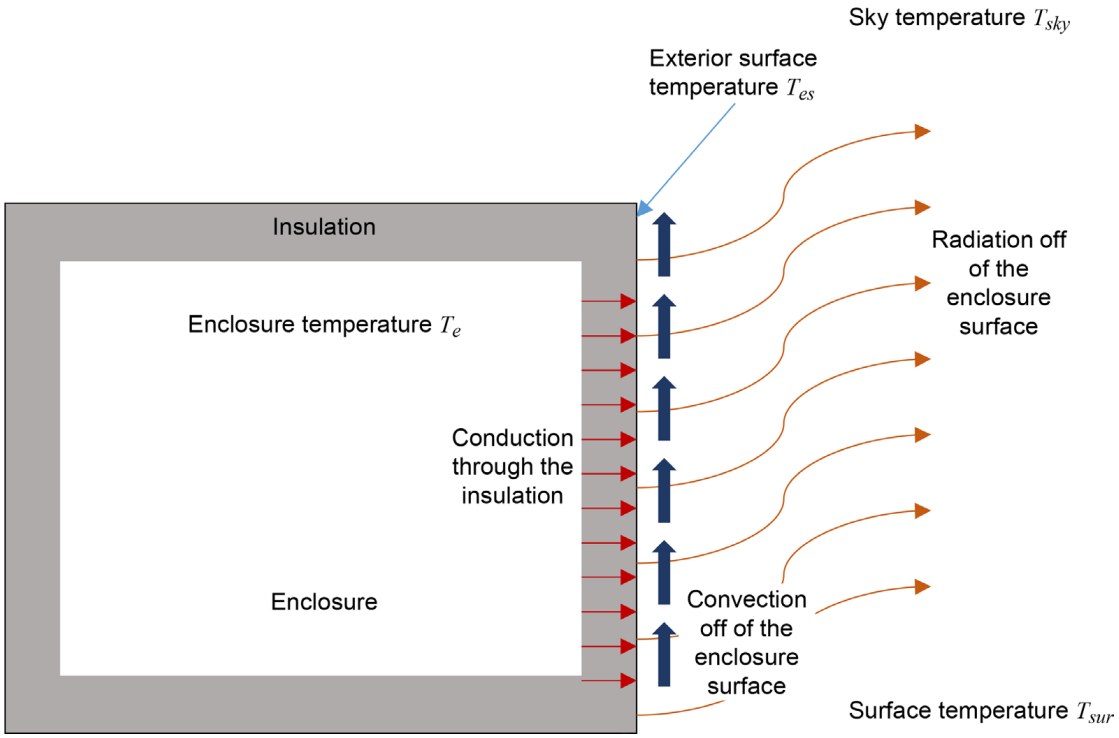

Figure 14.—Heat transfer from the enclosure to the surroundings.

Where the heat flow through the insulation is given by Equation (25) and is based on the temperature difference between the enclosure interior (T_{ei}) and the exterior surface (T_{es}), the enclosure area (A_e), the thermal conductivity (k_i) of the insulation and its thickness (t_i).

$$Q_e = \frac{A_e k_i \left(T_{ei} - T_{es}\right)}{t_i} \tag{25}$$

The convective (Q_{ec}) and radiative (Q_{er}) heat transfer from the enclosure to the surroundings are given by Equations (26) and (27), respectively. Equations (24) to (27) are solved iteratively to determine the enclosure surface temperature for a given internal enclosure temperature. Once this is determined, the heat loss through the insulation can be calculated from Equation (25). The heat loss through the insulation is then compared to the total waste heat generated within the enclosure. If they differ then the internal temperature is adjusted and the iterative process is repeated until the waste heat equals the heat loss. This process is illustrated in Figure 15.

$$Q_{ec} = A_e h\left(T_{es} - T_{sur}\right) \tag{26}$$

The convective coefficient is determined from Equation (11) where the characteristic length is the length of the enclosure.

$$Q_{er} = A_e \varepsilon \sigma \left[F_{esky}\left(T_{es}^4 - T_{sky}^4\right) + F_{esur}\left(T_{es}^4 - T_{sur}^4\right)\right] \tag{27}$$

The sky and surface temperatures are the same those for the radiator but the surface (F_{esur}) and sky (F_{esky}) view factors may be different for the enclosure then the radiator depending on its mounting location on the surface platform.

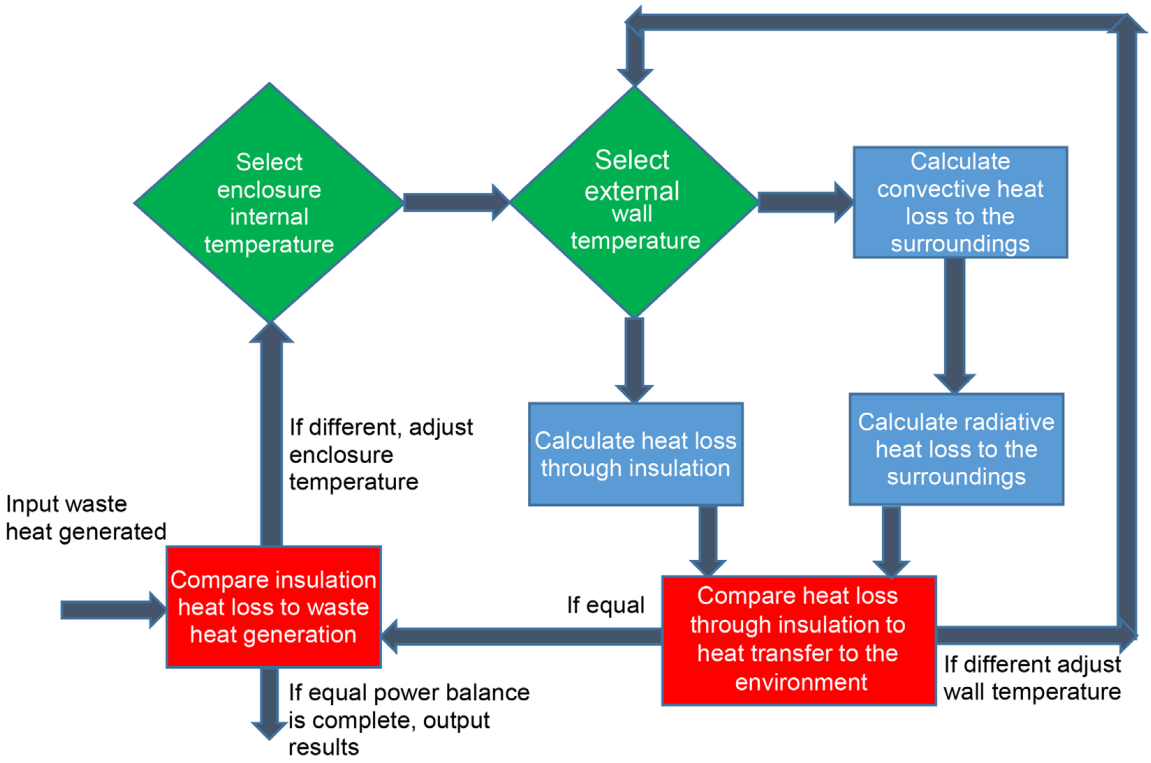

Figure 15.—Iterative process for calculating the enclosure internal temperature.

3.3 Heat Exchangers

To increase the efficiency of the solid oxide fuel cells, a number of heat exchanges will be utilized in order to use the waste heat produced to preheat the reactant gasses prior to them entering the fuel cell stack, as illustrated in Figure 3. A counter flow heat exchanger would be the best choice for achieving high efficiency heat transfer between two isolated fluids (Ref. 20). In a counter-flow heat exchanger, the incoming fluid flows in the opposite direction as the exiting fluid. A typical construction for this type of heat exchanger is to utilize a tube in tube design. Where the inner tube carries the hot fluid away from the heated source and the outer tube carries the cooler fluid entering the heat source. This is illustrated in Figure 16. To enhance the heat transfer between the tubes, fins can be added to either the inner tube or outer tube flow as shown in Figure 17. An example of the inlet and outlet arrangement for a tube-in-tube heat exchanger is also shown in Figure 18.

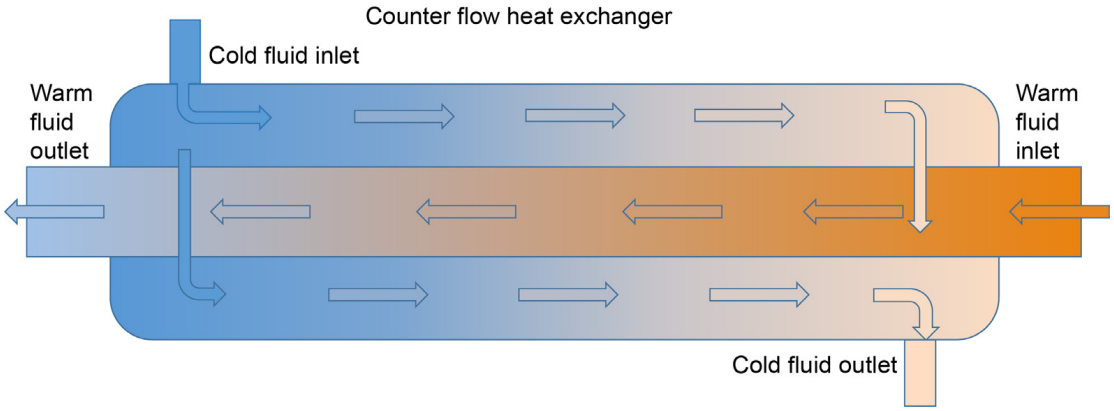

Figure 16.—Illustration of a counter flow heat exchanger (Ref. 20).

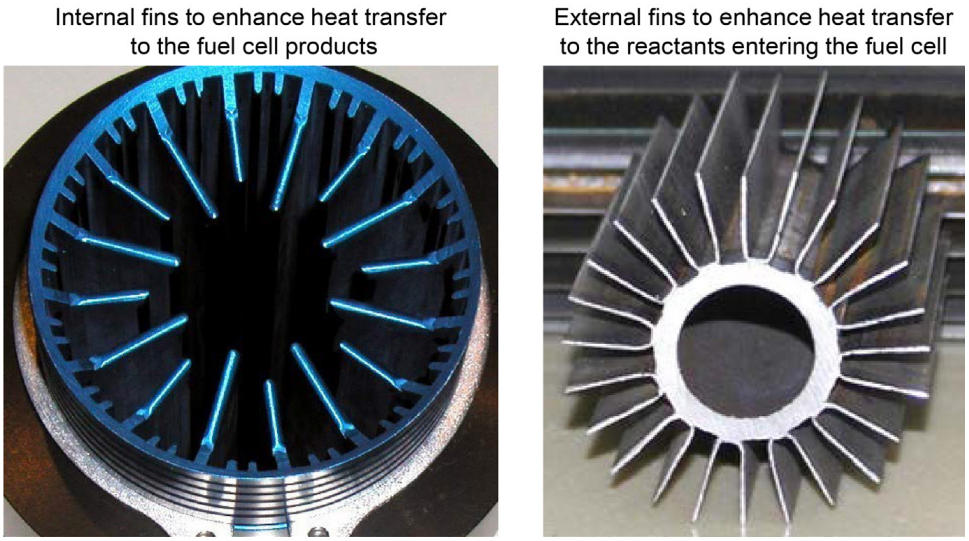

Figure 17.—Internal and external fins for enhancing heat transfer (Refs. 20 and 21).

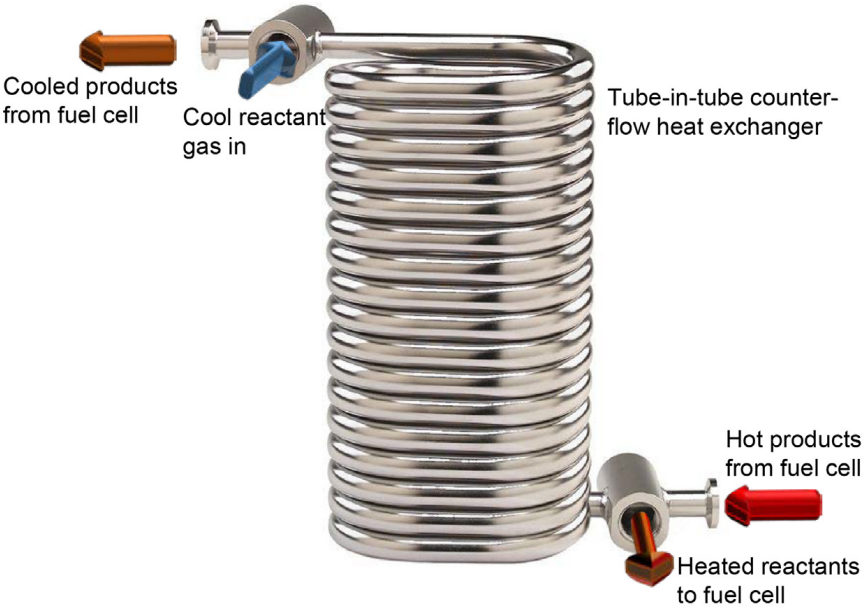

Figure 18.—Example of a tube-in-tube heat exchanger (Ref. 22).

A description of the analysis for sizing a heat exchanger for preheating the reactants as they enter the fuel cell with the byproduct fluid leaving the fuel cell is given in detail in Reference 20. The advantage of preheating the reactants is that, for a high temperature solid oxide fuel cell, it minimizes the parasitic heater power required to maintain a minimal temperature gradient across the fuel cell stack. Using unheated reactants stored at ambient conditions would introduce destructive thermal gradient within the fuel cell stack as the relatively cold reactants enter the hot fuel cell. This gradient would impact the fuel cell performance and introduce thermally induced mechanical stresses within the stack reducing its operational lifetime. Therefore, for the heat exchanger to be beneficial it needs to raise the temperature of the reactants to level as close as possible to the fuel cell operating temperature. The tradeoff in the ability to accomplish this is in the size of the heat exchanger as well as its overall effectiveness.

The properties of the reactant gasses, viscosity (μ_h, μ_o), specific heat (C_{ph}, C_{po} and thermal conductivity (k_h, k_o), are needed to accurately size the heat exchanger. Polynomial curve fits of these properties relative to the gas temperature were generated from data tables (Ref. 7 and 23). to be used in the heat exchanger sizing. These are given in Equations (28) to (33) and are plotted in Figure 19 to Figure 21.

$$\mu_h = 8.4584\times10^{-6} + 1.8724\times10^{-8}T_h - 3.6755\times10^{-12}T_h^2 \quad [\text{Pa·s}] \tag{28}$$

$$\mu_o = 1.9361\times10^{-5} + 5.2829\times10^{-8}T_o - 1.7735\times10^{-12}T_o^2 \quad [\text{Pa·s}] \tag{29}$$

$$C_{ph} = 13.359 + 2.0184\times10^{-3}T_h - 1.2506\times10^{-7}T_h^2 \quad [\text{kJ/kg·K}] \tag{30}$$

$$C_{po} = 0.89466 + 2.0184\times10^{-3}T_h - 1.2506\times10^{-7}T_h^2 \quad [\text{kJ/kg·K}] \tag{31}$$

$$k_h = -0.00525 + 7.856\times10^{-4}T_h - 4.90\times10^{-7}T_h^2 \quad [\text{W/m·K}] \tag{32}$$

$$k_o = 0.00048 + 9.2414\times10^{-5}T_h - 2.2143\times10^{-8}T_h^2 \quad [\text{W/m·K}] \tag{33}$$

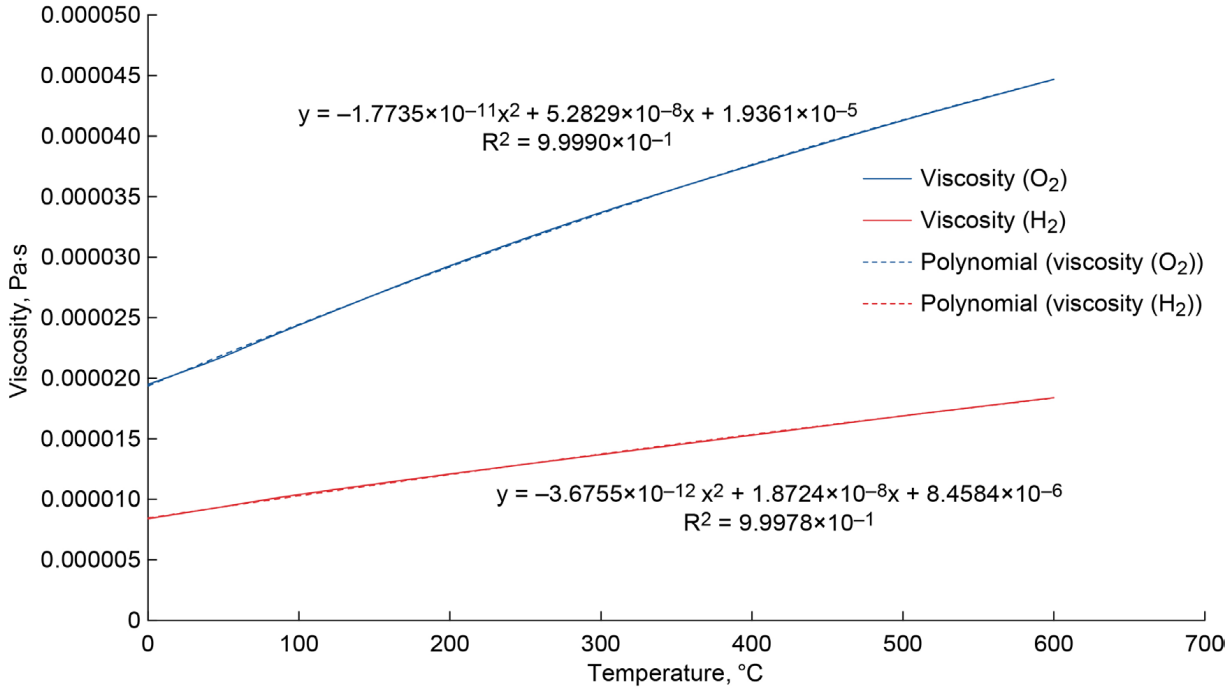

Figure 19.—Viscosity of hydrogen and oxygen as a function of temperature.

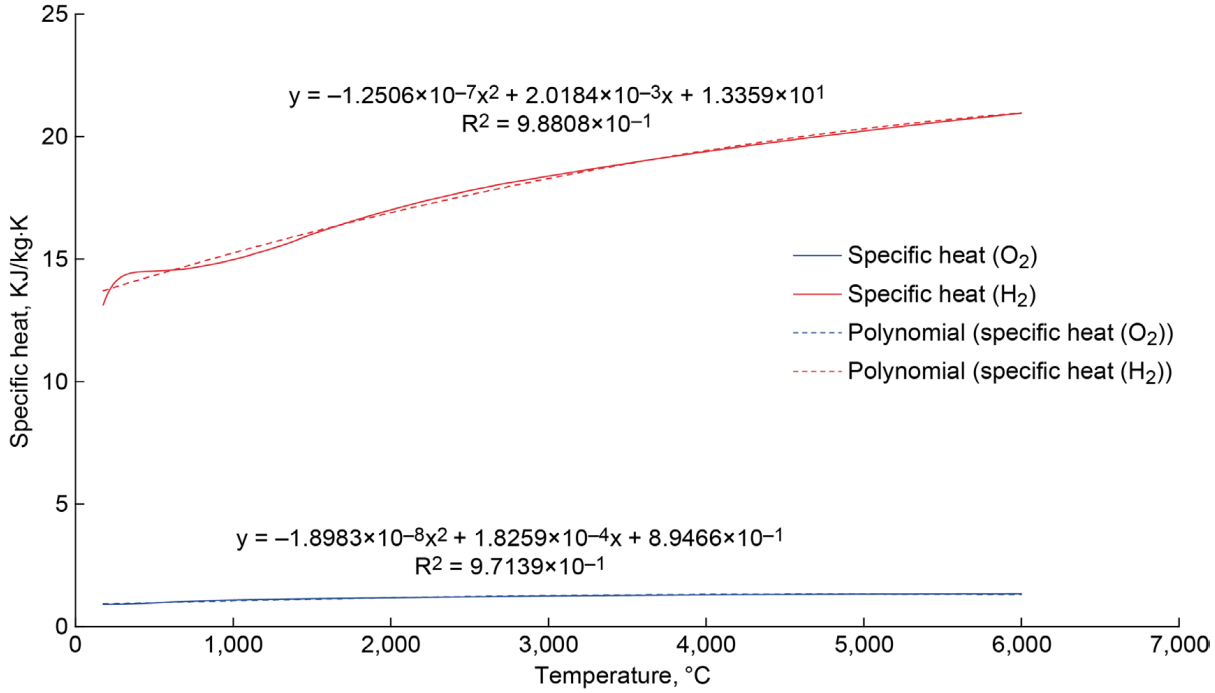

Figure 20.—Specific heat of hydrogen and oxygen as a function of temperature.

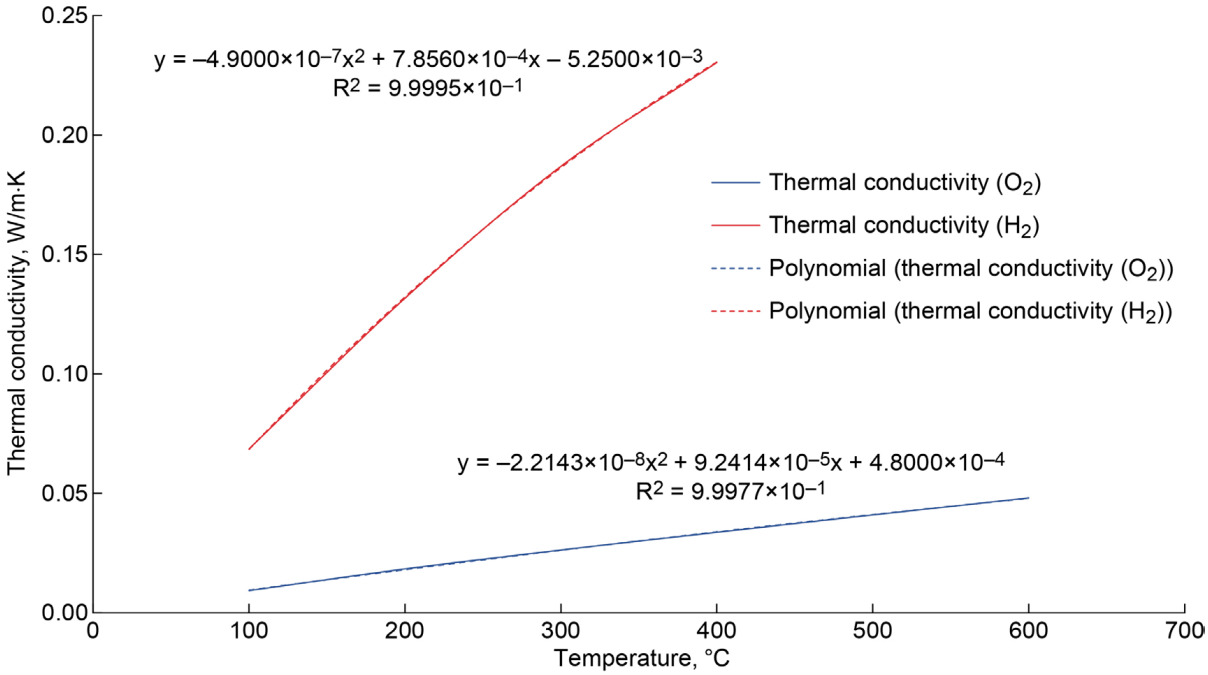

Figure 21.—Thermal conductivity of hydrogen and oxygen as a function of temperature.

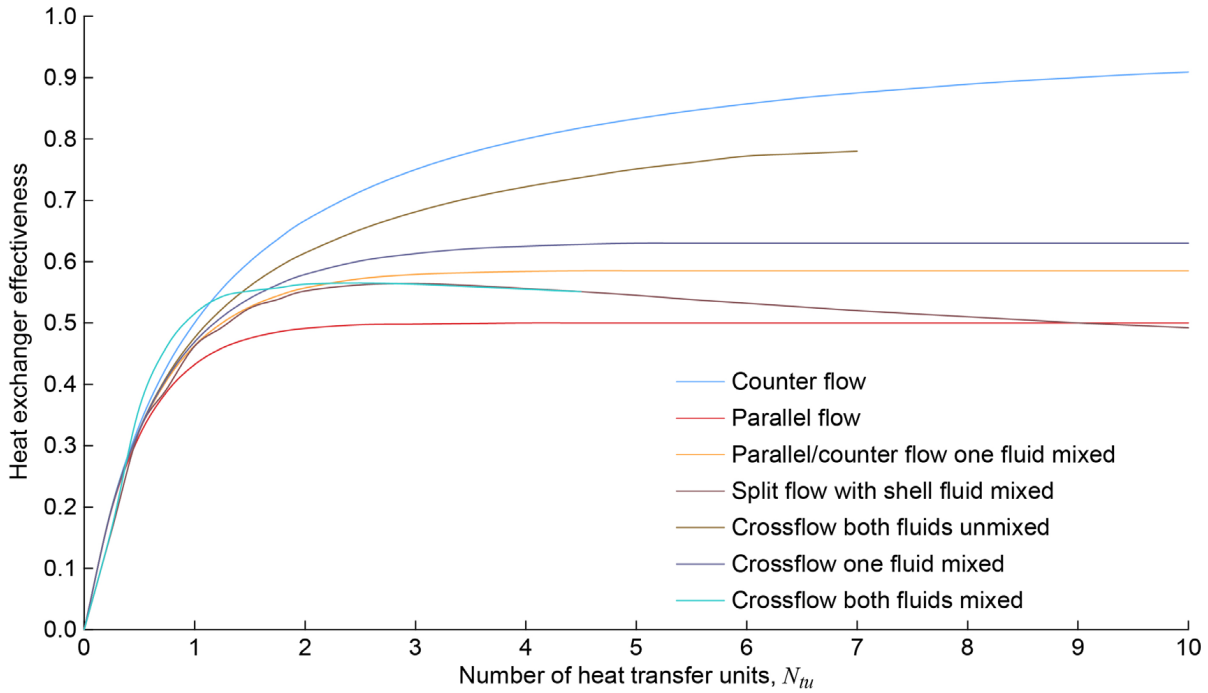

Figure 22.—Achievable heat exchanger effectiveness as a function of number of heat transfer units (Ref. 20).

A heat exchanger effectiveness of around 90 percent is achievable with a counter-flow type heat exchanger design as shown in Figure 22. This figure shows the theoretical heat exchanger effectiveness as a function of the heat transfer units of the heat exchanger. The number of heat transfer units (N_{tu}) is a nondimensional quantity, given by Equation (34), that expresses the heat transfer capability of the heat exchanger. This nondimensional quantity is based on the heat transfer area (A {m^2}), the thermal

conductance from one fluid to the next within the heat exchanger (U\{W/m^2·K\}) and the fluid capacity rate (C, \{W/K\}) which is the fluid mass flow ($\dot{m}$) multiplied by its specific heat at constant pressure (c_p) as given by Equation (35).

$$N_{tu} = \frac{AU}{C} \tag{34}$$

$$C = \dot{m} c_p \tag{35}$$

The greater the number of heat transfer units the higher the effectiveness of the heat exchanger up to its theoretical limit. The number of heat transfer units required by the heat exchanger would be around 9 or greater. Although a heat exchanger of this type of performance is feasible, the heat exchanger design would need to be developed and optimized for the specific fuel cell operation in order to achieve the high effectiveness value required.

The goal of the heat exchanger sizing is to raise the temperature of the reactants to within 150 °C of the fuel cell operating temperature of the solid oxide fuel cell after passing through the heat exchanger. This temperature was chosen as the starting point for the analysis and was selected as a reasonable inlet temperature to achieve through the use of the heat exchanger. The higher the inlet reactant temperature the larger and or more effective the heat exchanger needs to be to achieve this temperature. Selecting a reactant inlet temperature that is too close to the fuel cell operating temperature would result in an excessively large heat exchanger whose mass would become a driving factor in the system design. The 150 °C difference between the inlet and operating temperature raises the reactants to approximately 80 percent of the fuel cell operating temperature. The flow into and out of the fuel cell and heat exchanger is illustrated in Figure 23. Assuming an inlet reactant temperature (T_1) of 22 °C and a byproduct heat exchanger inlet temperature (T_3) of 900 °C, the achievable reactant inlet temperature to the fuel cell (T_2) is shown in Figure 21. This figure shows that to raise the reactant inlet temperature to the fuel cell to within 150 °C of its operating temperature will require a heat exchanger effectiveness of 0.9 or higher. Figure 24 shows that this is achievable with a counter flow design with 9 or more heat transfer units.

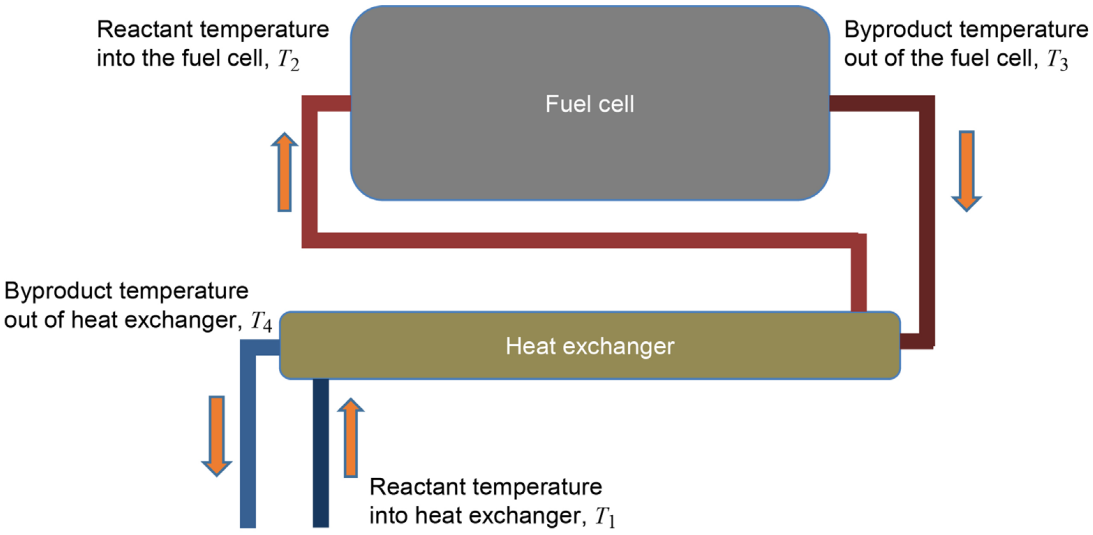

Figure 23.—Illustration of reactant and byproduct flow between the fuel cell and heat exchanger.

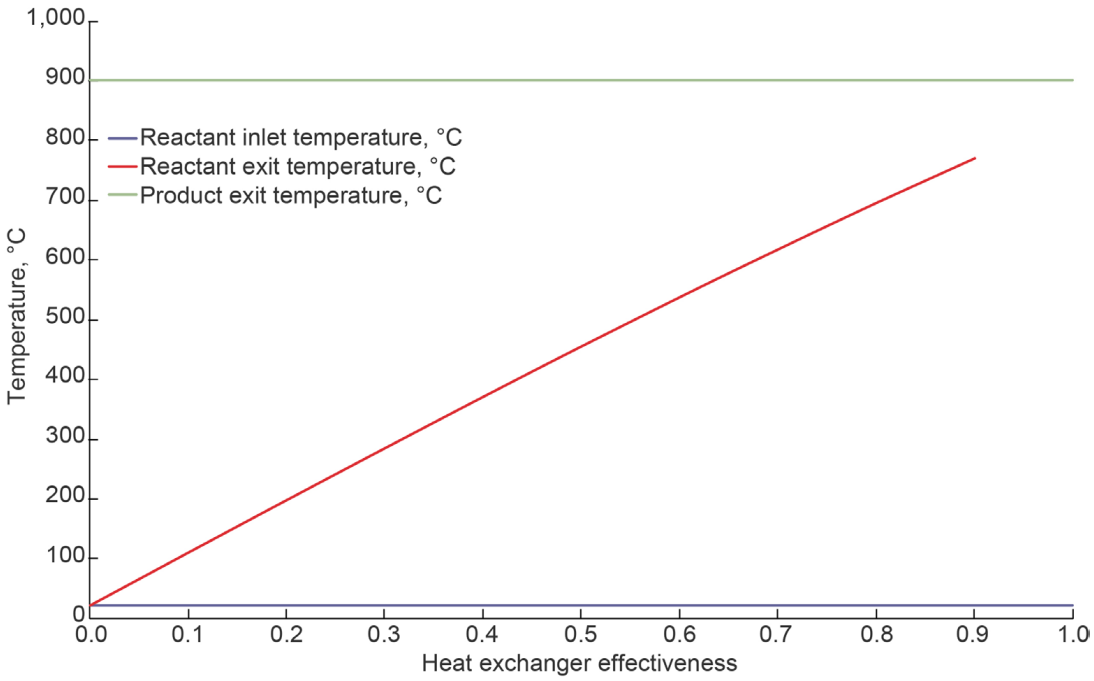

Figure 24.—Reactant temperature increase versus heat exchanger effectiveness.

4.0 Sizing Results

Using the analysis described in Section 3.0, a thermal system sizing was performed for the two types of fuel cell systems, PEM and solid oxide, at two different locations, one near the equator at 4.36° S latitude and one nearer the poles at 47.97° N latitude. These locations were chosen because environmental data from the MSL curiosity rover and Viking II lander, respectively, are available.

For all cases, it is assumed that the total required enclosed volume for both the fuel cell and balance of plant components is 1 m^3 (0.5 m^3 for the fuel cell and 0.5 m^3 for the balance of plant components). The overall thermal system mass sizing results for the PEM and solid oxide systems are shown in Figure 25. This figure shows that the PEM thermal system mass was greater than that for the solid oxide fuel cell. The main difference is in the size of the radiator. Because the solid oxide system is able to reject heat at a much higher temperature then the PEM system its radiator mass is significantly smaller. The thermal system balance of plan mass for the solid oxide system was greater than that of the PEM system as well as the insulation mass. This is also due to the higher operating temperature of the SO system over the PEM system. The SO system also required a heat exchanger which is not needed with the PEM system. A detailed summary of the results for the PEM and SO systems are given in Sections 4.1 and 4.2, respectively.

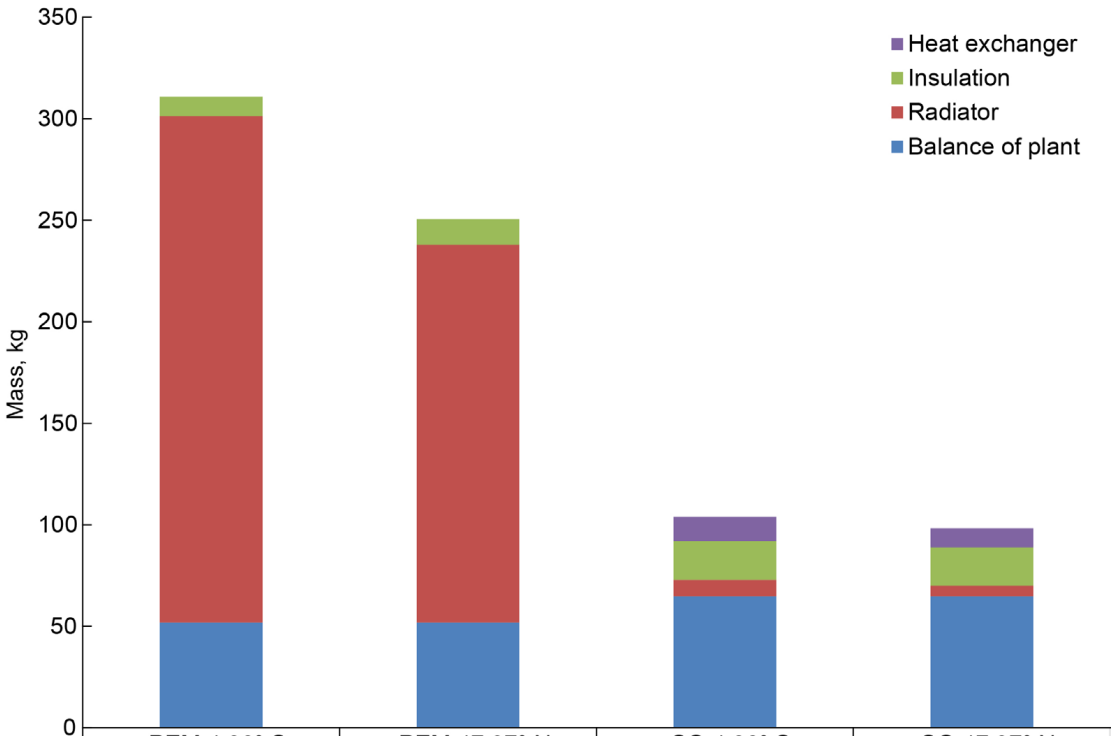

	PEM 4.36° S	PEM 47.97° N	SO 4.36° S	SO 47.97° N
Heat exchanger	0	0	12	9.2
Insulation	9.6	12.7	19	19
Radiator	249.3	186	8.04	5.13
Balance of plant	51.9	51.9	64.8	64.8

Figure 25.—Thermal system mass for proton exchange membrane (PEM) and solid oxide (SO) fuel cell system and operating latitude on Mars.

4.1 PEM Fuel Cell Thermal System Sizing Result

For the PEM fuel cell cases, the balance of plant and the fuel cells operate at nearly the same temperature (300 and 350 K, respectively) and therefore can be placed within the same enclosure. The total enclosure volume for both the fuel cell and balance of plant is estimated to be 1 m^3. The layout for the PEM fuel cell system is illustrated in Figure 26. The coolant selected for use with the PEM system is deionized water to avoid corrosion issues. This coolant is liquid over a larger temperature range than the design operating range of the PEM fuel cell thermal system. It is estimated that the coolant loop will require 10 L of the coolant.

The balance of plant components size with the fuel cell power level. For a 10-kW output fuel cell the balance of plant components and their associate masses are given in Table X.

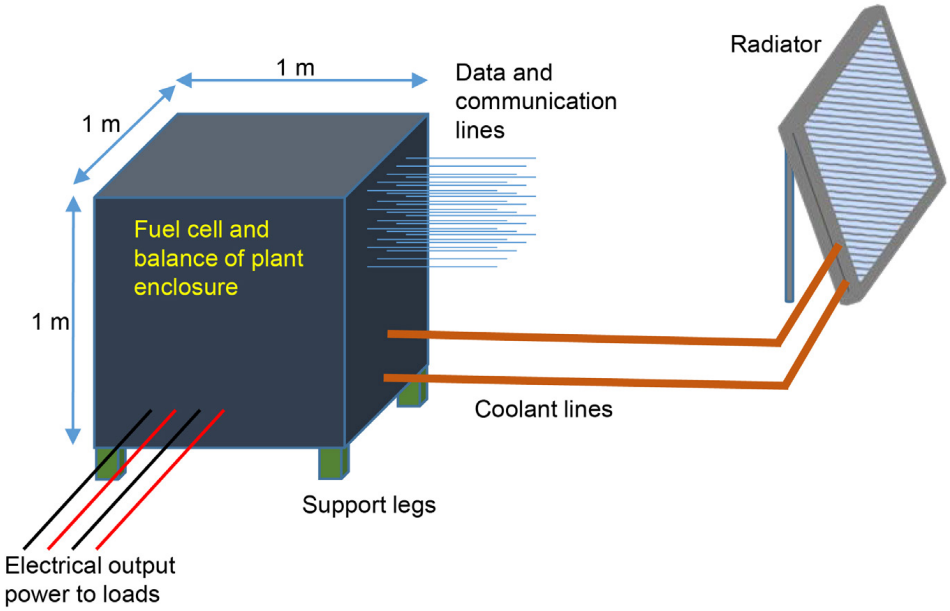

Figure 26.—Simplified PEM fuel cell and radiator layout.

TABLE X.—PEM FUEL CELL RADIATOR SYSTEM
BALANCE OF PLANT MASS ESTIMATES

Component	Mass, kg	Quantity	Total mass, kg
Flow control valve	1.5	1	1.5
Check valve	0.3	7	2.1
Vent/pressure relief valve	0.5	2	1
Servo valve	0.5	5	2.5
Coolant pump	6.75	2	13.5
Filter	0.4	2	0.8
Accumulator	5.4	2	10.8
Temperature sensor	0.1	3	0.3
Pressure sensor	0.1	6	0.6
Flow sensor	0.6	5	3.0
Coolant lines	0.53 (kg/m)	5 (m)	2.65
Cold plates	0.55	5	2.75
Coolant	1.04 (kg/l)	10 (l)	10.4
Total			51.9

The radiator will be sized for the worst case warm conditions and the insulation will be sized for the worst case cold conditions. The inputs and results for the radiator sizing are given in Table XI for both operating locations. The total heat to be rejected by the radiator consists of the waste heat generated by the fuel cell minus the heat loss from the fuel cell enclosure. Since the radiator is sized for the worst case warm conditions the heat loss from the enclosure is calculated based on those conditions.

TABLE XI.—RADIATOR SIZING RESULTS FOR PEM FUEL CELL SYSTEM

Input or variable	4.36° S location	47.97° N location
Sky temperature, K	192	179.5
Surface temperature, K	281	250
Enclosure temperature, K	300	300
Radiator temperature, K	300	300
Radiator view factor to the surface	0.5	0.5
Radiator view factor to the sky	0.5	0.5
Radiator panel emissivity	0.84	0.84
Wind speed (minimum), m/s	0.0	0.0
Convective coefficient (natural convection), $W/m^2 \cdot K$	0.11	0.15
Calculated radiative heat transfer, W/m^2	204.7	268.1
Calculated convective heat transfer, W/m^2	2.1	7.5
Waste heat to be rejected, kW	6.6	6.56
Radiator area, m^2	31.9	23.8
Radiator mass, kg	249.3	186.0

TABLE XII.—INSULATION SIZING RESULTS FOR PEM FUEL CELL SYSTEM

Input or variable	4.36° S location	47.97° N location
Sky temperature, K	152.3	139.7
Surface temperature, K	185	155
Enclosure temperature, K	300	300
Insulation thermal conductivity, W/m·K	0.017	0.017
Insulation density, kg/m^3	20	20
Enclosure view factor to the surface	0.5	0.5
Enclosure view factor to the sky	0.5	0.5
Enclosure surface emissivity	0.5	0.5
Wind speed (maximum average), m/s	4.4	4.4
Convective coefficient (natural convection), $W/m^2 \cdot K$	0.72	0.75
Calculated radiative heat transfer, W/m^2	15.2	9.97
Calculated convective heat transfer, W/m^2	5.9	11.0
Enclosure surface temperature, K	193.1	166.5
Heat loss through the insulation, W	126.9	126.0
Heat loss through the support legs, W	37.0	46.6
Heat loss through the data wires (25 wires), W	5.0	5.5
Heat loss through the power wires (4 wires), W	19.9	22.0
Total heat loss, W	200	200
Insulation thickness, cm	8.0	10.6
Insulation mass, kg	9.6	12.7

The insulation sizing and maximum heat loss from the enclosure is determined based on the worst case cold conditions at each location. The heat loss is calculated through the insulation as well as items that pass through the insulation to the external environment. The exterior of the enclosure was assumed to be covered in metallic paint which has an emissivity of 0.5 (Ref. 24). The assumed pass-throughs include 4 support legs for raising the enclosure off of the surface, 25 data and or communications wires and 4 power wires. Although the heat pipes also pass through the insulation they are considered part of the radiator system and do not count toward the miscellaneous heat loss from the enclosure. Also, it was assumed that the internal waste heat generation from the balance of plant components was 300 W. Therefore, the insulation was sized to limit the heat loss to the surroundings from the enclosure to below the 300 W waste heat generation. The insulation sizing results are given in Table XIII.

4.2 Solid Oxide Fuel Cell Thermal System Sizing Result

For the solid oxide fuel cell cases, there is a significant difference between the operating temperature of the fuel cells (1,023 K) and the balance of plant (300 K). Therefore, the enclosure volume is split into two sections of 0.5 m^3 each as illustrated in Figure 27. The balance of plant components are similar to those for the PEM system. The primary difference is the addition of the recuperative heat exchangers to recover some of the waste heat from the reactor to preheat the reactants prior to entering the fuel cell. The coolant selected for use with the solid oxide system is a lithium. This coolant is liquid over a temperature range that is larger than the design operating range of the solid oxide fuel cell thermal system. It is estimated that the coolant loop will require 5 L of the coolant. This is less than the volume of coolant used with the PEM system due to the smaller radiator size needed with the solid oxide fuel cell system.

The balance of plant electronics and components will operate at a lower temperature then the solid oxide fuel cell. This temperature will be similar to that of the PEM system at 300 K. Therefore, a second

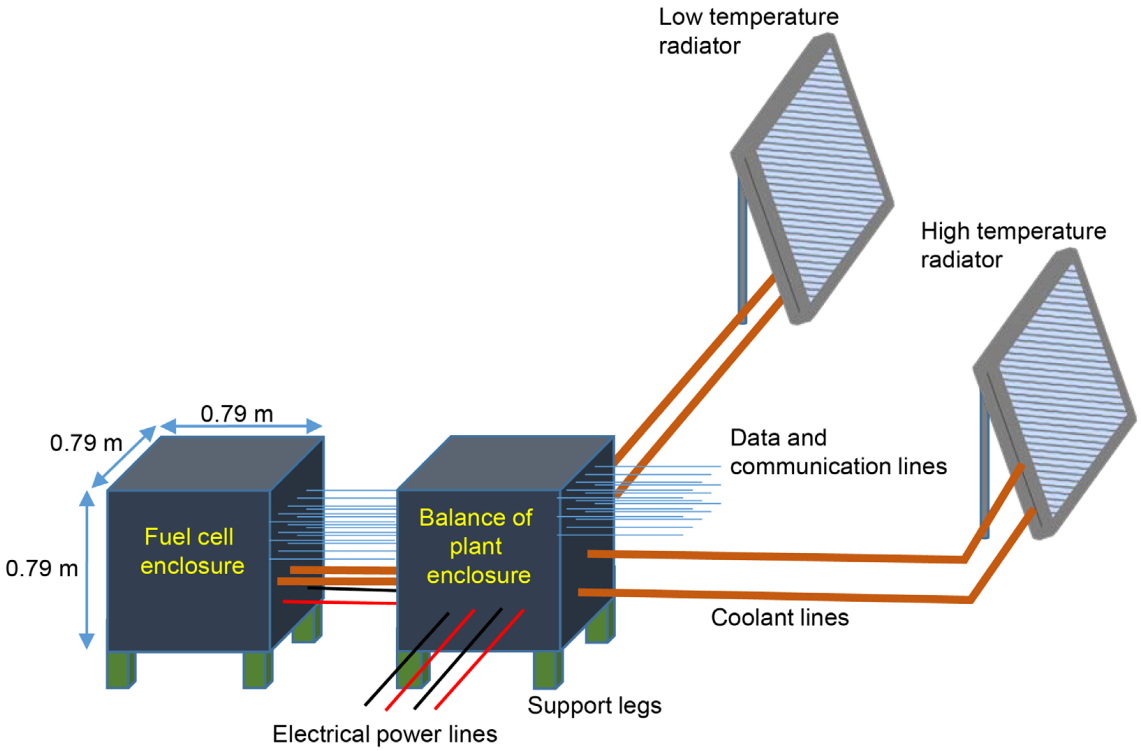

Figure 27.—Simplified solid oxide fuel cell and radiator layout.

TABLE XIII.—SOLID OXIDE FUEL CELL RADIATOR SYSTEM BALANCE OF PLANT MASS ESTIMATES

Component	Mass, kg	Quantity	Total mass, kg
Flow control valve	2.25	1	2.25
Check valve	0.45	7	3.15
Vent/pressure relief valve	0.75	2	1.5
Servo valve	0.75	5	3.75
Coolant pump	10.125	2	20.25
Filter	0.6	2	1.2
Accumulator	8.1	2	16.2
Temperature sensor	0.15	3	0.45
Pressure sensor	0.15	6	0.9
Flow sensor	0.9	5	4.5
Coolant lines	0.8 (kg/m)	5 (m)	4
Cold plates (low temperature)	0.55	5	2.75
Heat pipes (low temperature)	0.15	10	1.5
Coolant	0.48 (kg/l)	5 (l)	2.4
		Total	64.8

low temperature radiator will be needed to reject the excess heat from these components. The assumed heat load of the balance of plant components is similar to that of the PEM system at 300 W. This low temperature heat rejection system will use heat pipes and cold plates to move the waste heat from the components to the radiator.

The balance of plant components size with the fuel cell power level. For a 10-kW output fuel cell the balance of plant components and their associate masses are given in Table XIII. Since representative components that can operate at the high temperature of the solid oxide fuel cell are not readily available, the mass of all of the PEM balance of plant components, except the cold plates and coolant, was increased by 50 percent to account for additional material and insulation to operate at the higher solid oxide temperatures.

The low and high temperature radiators will be sized for the worst-case warm conditions and the insulation will be sized for the worst-case cold conditions. The inputs and results for both the low and high latitude radiator sizing are given in Table XIV for both operating locations.

The insulation sizing and maximum heat loss from the enclosure is determined based on the worst-case cold conditions at each location. For the solid oxide system, there are two enclosures; one containing the electronics and balance of plant components and the other containing the fuel cell stacks and other high-temperature components. Since the electronics/BoP enclosure has its own dedicated radiator to reject the waste heat, the insulation on this enclosure is set at a fixed amount to minimize heat loss during the worst-case cold operating conditions. The heat loss is calculated through the insulation as well as items that pass through the insulation to the external environment. The assumed pass-throughs for each enclosure include four support legs for raising the enclosures off of the surface, 45 data/communications wires from the electronics/BoP enclosure and 20 data/communication wires from the fuel cell enclosure and six power wires in the electronics/BoP enclosure and two power wires for the fuel cell enclosure. The insulation sizing results are given in Table XV.

TABLE XIV.—RADIATOR SIZING RESULTS FOR SOLID OXIDE FUEL CELL SYSTEM

Input or variable	4.36° S location		47.97° N location	
Radiator application	Electronics/ BoP	Fuel cell	Electronics/ BoP	Fuel cell
Sky temperature, K	192	192	179.5	179.5
Surface temperature, K	281	281	250	250
Enclosure temperature, K	300	1,023	300	1,023
Radiator temperature, K	300	1,023	300	1,023
Radiator view factor to the surface	0.5	0.5	0.5	0.5
Radiator view factor to the sky	0.5	0.5	0.5	0.5
Radiator panel emissivity	0.84	0.84	0.84	0.84
Wind speed (minimum), m/s	0.0	0.0	0.0	0.0
Convective coefficient (natural convection), $W/m^2 \cdot K$	0.18	0.55	0.24	0.57
Calculated radiative heat transfer, W/m^2	204.7	51,984	268.1	52,048
Calculated convective heat transfer, W/m^2	3.4	411.0	12.2	438.5
Waste heat to be rejected, W	300	2,265	300	2,237
Radiator area, m^2	1.0	0.04	0.61	0.04
Radiator mass, kg	7.7	0.34	4.8	0.33

TABLE XV.—INSULATION SIZING RESULTS FOR SOLID OXIDE FUEL CELL SYSTEM

Input or Variable	4.36° S Location		47.97° N Location	
Enclosure	Electronics/ BoP	Fuel Cell	Electronics/ BoP	Fuel Cell
Sky temperature, K	152.3	152.3	139.7	139.7
Surface temperature, K	185	185	155	155
Enclosure temperature, K	300	1,023	300	1,023
Insulation thermal conductivity, W/m·K	0.017	0.017	0.017	0.017
Insulation density, kg/m^3	20	20	20	20
Enclosure view factor to the surface	0.5	0.5	0.5	0.5
Enclosure view factor to the sky	0.5	0.5	0.5	0.5
Wind speed (maximum average), m/s	4.4	4.4	4.4	4.4
Convective coefficient (natural convection), $W/m^2 \cdot K$	0.89	0.89	0.91	0.91
Calculated radiative heat transfer, W/m^2	13.4	78.5	9.5	66.1
Calculated convective heat transfer, W/m^2	5.19	53.8	12.7	68.7
Enclosure surface temperature, K	190.8	245.3	168.9	230.3
Heat loss through the insulation, W	88.1	627.6	105.7	639.8
Heat loss through the support legs, W	37.0	269.6	46.7	279.3
Heat loss through the data wires, W	4.28	42.2	5.8	43.7
Heat loss through the power wires, W	17.13	168.9	23.2	175.0
Total heat loss, W	146.5	1,108.4	181.4	1,137.7
Insulation thickness, cm	10	10	10	10
Insulation mass, kg	9.5	9.5	9.5	9.5

The insulation thickness of 10 cm was selected for both enclosures because it met the key characteristics for both enclosures. For the electronics/BoP enclosure under the worst-case cold operating conditions, this insulation thickness kept the heat loss below the waste heat generated within the box. Thus, this conservative approach always requires radiators and does not require heaters to maintain the internal temperature if the equipment within the enclosure is operational. For the fuel cell enclosure, this level of insulation kept the external wall temperature below 300 K which was the desired upper limit of the wall temperature to minimize temperature gradients within the enclosure.

The possibility of not utilizing a coolant loop and radiator with the high temperature solid oxide fuel cell enclosure was also considered. Under these conditions the insulation would be sized to reject the full 3,330 W of excess heat through the walls of the enclosure. Two approaches to this were evaluated. The first is that the excess heat is rejected somewhat uniformly through all of the walls of the enclosure. The insulation thickness is the same on all of the walls. The second option is to reduce the insulation thickness on the top surface allowing the majority of the heat to be released from this surface. The results from this approach to rejecting heat from the fuel cell enclosure are given in Table XVI.

In both of these cases, the waste heat can be radiated from the enclosure directly by reducing the insulation thickness within the enclosure. However, there are a number of drawbacks to this approach. The main concern is that radiating the waste heat directly from the enclosure will produce a temperature gradient within the fuel cell stack. This is especially true for the second case where the majority of the waste heat is rejected from only one side of the enclosure. A temperature gradient within the fuel cell stack will reduce its operating efficiency as well as introduce thermally induced mechanical stresses to the solid oxide stack materials potentially reducing the operational lifetime of the fuel cell. Another concern is that the surface temperature of the enclosure will be considerably higher than the surroundings. This will reradiate to surrounding equipment as well as the electronics enclosure. The preferred method for removing the waste heat from the solid oxide fuel cell enclosure is to utilize a radiator. Although the radiator size is small and it adds additional components to the system, removing the waste heat in this controlled manner enables better control of the internal temperature of the fuel cells which is critical to its operation and lifetime.

To recapture as much of the waste heat as possible from the products and to preheat the reactants, recuperative heat exchangers were sized for both the inlet oxygen and hydrogen reactant flow lines. As identified in Section 3.0, the heat exchangers were a counter flow design with an effectiveness of 0.9 and requiring 9 thermal heat transfer units. The sizing results for these heat exchangers is given in Table XVII. Nickel was chosen as the heat exchanger material. Nickel has a high melting temperature of 1,455 °C and is resistant to hydrogen embrittlement. However, there is a concern that Nickel will react with the CO_2 gas at high temperatures. Even though the atmosphere is rarified it may be necessary to utilize a different heat exchanger material if issues with the atmosphere interacting with the heat exchanger become evident.

TABLE XVI.—REJECTION OF WASTE HEAT THROUGH THE FUEL CELL ENCLOSURE

Location	Thickness, cm	Temperature		Internal power, W	Heat loss through insulation, W
		Internal, K	Surface, K		
Fuel cell (all surfaces covered with same insulation level)	2.4	1,023	372	3,330	2,189
Fuel cell upper surface insulation (reduced to radiate heat)	0.2	1,023	580	3,330	2,298

TABLE XVII.—HEAT EXCHANGER SIZING FOR HYDROGEN AND OXYGEN REACTANTS

Parameter	Oxygen	Hydrogen
Reactant inlet temperature to the heat exchanger, °C	22	22
Byproduct inlet temperature to the heat exchanger, °C	750	750
Reactant exit temperature from the heat exchanger, °C	646	653
Byproduct exit temperature from the heat exchanger, °C	95	95
Flow rate, L/min	82.4	165.7
Average viscosity, Pa-s	0.975	3.33×10^{-5}
Average specific heat, J/kg-K	14,214	14,263
Average thermal conductivity, W/m-K	0.253	0.0623
Required heat exchanger area, m^2	0.38	0.29
Inner tube diameter, cm	1	1
Outer tube diameter, cm	2	2
Wall thickness, mm	1	1
Tube length, m	11.94	9.13
Heat exchanger material	Nickel	Nickel
Heat exchanger mass, kg	12.0	9.2

5.0 Summary

The thermal system sizing for both the proton exchange membrane (PEM) and solid oxide-based fuel cell power systems provided a mass estimate of the main components within the thermal control system. Systems were sized for two locations for both types of fuel cells. The locations represented near equator and high latitude operation.

The overall thermal system mass of the solid oxide fuel cell system was much less than that for the PEM fuel cell systems. This was driven mainly by the required radiator size for the PEM systems. The radiators for the PEM system operated at a much lower temperature then those for the solid oxide fuel cells. The lower operating temperature required much larger radiators and therefore a higher radiator mass. Because the radiator size was the dominant factor in the thermal system mass for the PEM fuel cells, the mission site had a significant effect on the overall PEM thermal system mass. Operating at higher latitudes where the worst-case hot temperatures were lower resulted in a smaller radiator size and therefore lower system mass. In contrast, the solid oxide thermal system showed a minor change in mass between operating locations due to the consistently large difference between rejection temperature and ambient temperatures. The balance of plant for the solid oxide system was the largest mass item. The mass for the balance of plant was greater than that for the PEM system due to the high temperature operation of the components.

References

1. Pilatowsky, I., Romero, R.J., Isaza, C.A. and Gamboa, S.A., “Cogeneration Fuel Cell-Sorption Air Conditioning Systems, Chapter 2: Thermodynamics of Fuel Cells,” Springer 978-1-84996-027-4, 2011.

2. Peters, R, Deja, R., Engelbracht, M., Frank, M., Nguyen, V.N., Blum, L. and Stolten, D., "Efficiency Analysis of a Hydrogen-Fueled Solid Oxide Fuel Cell System with Anode Off-Gas Recirculation," Journal of Power Sources, 328, 105-113, 2016.
3. Williams, D.R, "Mars Fact Sheet", NASA Goddard Space Flight Center, December 2016.
4. Vesovic, V., Wakeham, W.A., Olchowy, G.A., Sengers, J.V., Watson, J.T.R., Millat, J., "The Transport Properties of Carbon Dioxide," Journal of Physical and Chemical Reference Data, Vol 19, Issue 3, 1990.
5. The Engineering Toolbox web site, www.engineeringtoolbox.com, April 2017.
6. Chanover, N. and Huber L., NASA PDS: The Planetary Atmospheres Node, September 2016.
7. Tillman, J.E., Johnson, N.C. and LeCompte, G.F., Meteorology Data---Direct from Mars!, University of Washington, Web Site www-k12.atmos.washington.edu, April 2017.
8. Rover Environmental Monitoring Station (REMS), www.curiosityrover.com/rems/, April 2017.
9. Incropera F.P. and DeWitt, D.P., *Fundamentals of Heat and Mass Transfer*, Third Edition, John Wiley & Sons, 1990.
10. Paris, A.D., Bhandari, P and Birur G.C., "High Temperature Mechanically Pumped Fluid Loop for Space Applications—Working Fluid Selection," JPL Report 2004-01-2415.
11. Roser, R. Laird Engineering Thermal Systems, "Common Coolant Types and Their Uses in Liquid Cooling Systems," Thermal News, June 13, 2016.
12. National Refrigerants Inc., *Refrigerant Reference Guide: R-11 and R-12 Technical Guidelines*, 5th Edition 2010.
13. Solutia, Therminol 59 Technical Bulletin, January 1998.
14. Dow, Syltherm XLT Technical Data Sheet.
15. Angelo, J.A. and Buden D., *Space Nuclear Power*, Orbit Book Company, 1985.
16. U.S .Department of Energy, "Aerogel Insulation: The Materials Science of Empty Space," https://energy.gov/eere/amo/articles/aerogel-insulation-materials-science-empty-space, October 11, 2013.
17. Aerogel Technologies LLC., web site, http://www.buyaerogel.com, July 2017.
18. Colozza, A.J. and Burke, K.A., "Evaluation of a Passive Heat Exchanger Based Cooling System for Fuel Cell Applications," NASA/TM—2011-216962, January 2011.
19. PT. Global Metal Engineering, web site, http://www.gme.co.id/products/studded-finned-tube/finned, July 2017.
20. Exergy Heat Transfer Solutions, www.exergyllc.com, July 2017.
21. Engineers Edge web site, engineersedge.com, July 2017.
22. Drake, B.G., Editor, "Reference Mission Version 3.0 Addendum to the Human Exploration of Mars: The Reference Mission of the NASA Mars Exploration Study Team," NASA Special Publication 6107-ADD, EX13-98-036, June 1998.
23. Drake, B.G., Editor, "Human Exploration of Mars Design Reference Architecture 5.0," NASA/SP—2009-566, July 2009.
24. Gilmore, D.G., Stuckey W.K. and Fong, M. Spacecraft Thermal Control Handbook Chapter 4: *Thermal Surface Finishes*, The Aerospace Press, ISBN: 978-1-884989-11-7, 2002.